# Phenyl Ether- and Aniline-Containing 2-Aminoquinolines as Potent and Selective Inhibitors of Neuronal Nitric Oxide Synthase

Maris A. Cinelli,[†] Huiying Li,[‡] Anthony V. Pensa,[†] Soosung Kang,[†] Linda J. Roman,[§] Pavel Martásek,[§,∥,⊥] Thomas L. Poulos,*,[‡] and Richard B. Silverman*,[†]

[†]Department of Chemistry, Department of Molecular Biosciences, Chemistry of Life Processes Institute, Center for Molecular Innovation and Drug Discovery, Northwestern University, 2145 Sheridan Road, Evanston, Illinois 60208-3113, United States

[‡]Departments of Molecular Biology and Biochemistry, Pharmaceutical Sciences, and Chemistry, University of California, Irvine, California 92697-3900, United States

[§]Department of Biochemistry, University of Texas Health Science Center, San Antonio, Texas 78384-7760, United States

[∥]Department of Pediatrics, First Faculty of Medicine, Charles University, Prague, Czech Republic

[⊥]BIOCEV, Prague, Czech Republic

S *Supporting Information*

ABSTRACT: Excess nitric oxide (NO) produced by neuronal nitric oxide synthase (nNOS) is implicated in neurodegenerative disorders. As a result, inhibition of nNOS and reduction of NO levels is desirable therapeutically, but many nNOS inhibitors are poorly bioavailable. Promising members of our previously reported 2-aminoquinoline class of nNOS inhibitors, although orally bioavailable and brain-penetrant, suffer from unfavorable off-target binding to other CNS receptors, and they resemble known promiscuous binders. Rearranged phenyl ether- and aniline-linked 2-aminoquinoline derivatives were therefore designed to (a) disrupt the promiscuous binding pharmacophore and diminish off-target interactions and (b) preserve potency, isoform selectivity, and cell permeability. A series of these compounds was synthesized and tested against purified nNOS, endothelial NOS (eNOS), and inducible NOS (iNOS) enzymes. One compound, **20**, displayed high potency, selectivity, and good human nNOS inhibition, and retained some permeability in a Caco-2 assay. Most promisingly, CNS receptor counterscreening revealed that this rearranged scaffold significantly reduces off-target binding.
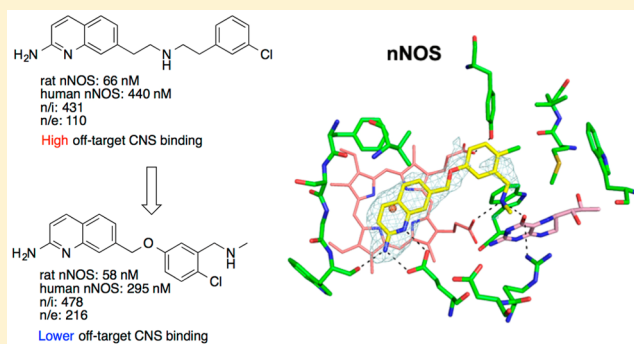
INTRODUCTION

Neurodegenerative disorders, such as Alzheimer's, Parkinson's, and Huntington's diseases, amyotrophic lateral sclerosis (ALS), and others, are diseases where the structure and function of neurons gradually deteriorate, leading to the motor, cognitive, and psychological difficulties associated with these disorders. Neuronal damage also occurs in head trauma, cerebral palsy, stroke, and ischemic events. With the world's increasingly aged population, the incidence of neurodegenerative disorders is also increasing, and, with most treatments limited to palliative care, the development of new therapeutics is of utmost importance.

A target receiving considerable attention is neuronal nitric oxide synthase (nNOS).[1] Nitric oxide (NO), an important second messenger, is produced by three nitric oxide synthase (NOS) enzymes: inducible nitric oxide synthase (iNOS), required for immune response activation, endothelial nitric oxide synthase (eNOS), which regulates blood pressure and vascular tone, and nNOS, necessary for neuronal signaling.[2] If nNOS is overexpressed or overactive in neuronal tissue, however, the excess NO, especially if converted to peroxyni-

trite, can cause free radical damage to cellular structures and protein nitration, which can lead to misfolding and aggregation.[3,4] Abnormally high levels of nNOS and NO have therefore been associated with or implicated in numerous neurodegenerative disorders,[5−8] making nNOS inhibition a desirable therapeutic avenue for the treatment or prevention of these conditions.[9−11]

Nitric oxide synthases are unique among mammalian enzymes in that they are homodimers requiring five cofactors to function: flavin adenine dinucleotide (FAD), flavin mononucleotide (FMN), and reduced nicotinamide adenine dinucleotide phosphate (NADPH), found in each monomer's reductase domain, and (6R)-5,6,7,8-tetrahydrobiopterin (H₄B) and the final electron acceptor, heme, which bind in each monomer's oxygenase domain along with the substrate, L-arginine. Between the two domains lies a flexible region where calmodulin binds when activated by calcium ion, and electron

flow proceeds from one monomer's reductase domain to the other's oxygenase domain,[12] where NO is produced as L-arginine is oxidized to L-citrulline.[13]

One important challenge in the design of nNOS inhibitors is that eNOS and iNOS, in sequence and overall structure, are nearly identical to nNOS, especially in their active site residues.[14,15] Nonselective NOS inhibition is potentially dangerous: iNOS inhibition could interfere with immune activation, while eNOS inhibition can cause severe hypertension and other cardiovascular liabilities.[16] Additionally, many nNOS inhibitors are mimics of L-arginine and thus have high basicity and polarity, large total polar surface area (tPSA), and many hydrogen bond donors, all of which hinder the inhibitors' blood−brain barrier (BBB) penetration and diminish therapeutic use.[17]

In 2014, we reported a series of 2-aminoquinolines as competitive nNOS inhibitors.[18] Two compounds, 1 and 2 (Figure 1), were considered promising candidates for further
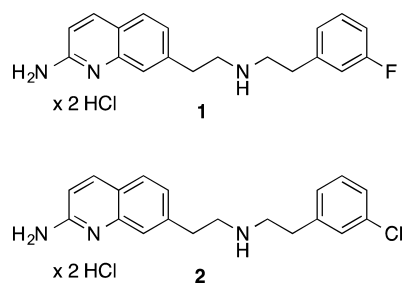
Figure 1. Aminquinoline-containing nNOS inhibitors 1 and 2.

development because of their high potency and selectivity over iNOS and eNOS. These compounds are permeable in a Caco-2 assay, and 1 displayed good oral bioavailability and brain permeation in mice. Although only modestly potent in vivo, 2 also inhibited nNOS in rat brain homogenates and in the brains of live rats. Despite their promise, 1 and 2 have major disadvantages. Compound 2 has a poor safety profile in rats, displaying toxic side effects at the doses required for effective nNOS inhibition. Furthermore, a counterscreen against a panel of relevant CNS targets and receptors performed by the Psychoactive Drug Screening Program (PDSP)[19] revealed that 1 and especially 2 are promiscuous binders with strong (<100 nM) affinities for serotonin, opioid, and histamine receptors, as well as for the dopamine and norepinephrine transporters, which could cause unfavorable side effects. Additionally, compounds 1 and 2 are quite time-consuming to synthesize (12 steps). Because of these problems, we chose to investigate alternative aminoquinoline-containing scaffolds for nNOS inhibition.

Interestingly, the literature revealed that compounds such as ketanserin, haloperidol, and risperidone, which also bind to multiple, similar CNS targets, have overall structural motifs in common with 1 and 2: two hydrophobic or aromatic exteriors (one, often halogenated), joined by an interior alkylamine linker, a pharmacophore (Figure 2A) that appears to "stick" to GPCRs and other CNS targets.[20]

Lowe and colleagues at Pfizer[21] reported the structure of 3, a potent nNOS inhibitor with very high affinity for dopamine and serotonin receptors. Removal of the exterior hydrophobic group diminished off-target binding, and when an exterior polar amine was attached to an interior hydrophobic group (such as in 4 and 5), higher potency and isoform selectivity resulted.[22,23] Similar exterior polar amines (especially N-methyl and N,N-dimethylamines) were also effective in conferring potency and selectivity of NeurAxon's thiophenecarboximidamides.[24,25]

Design of an analogous "inverted" aminoquinoline-containing compound (Figure 2B) resulted in 6, with the halves of the
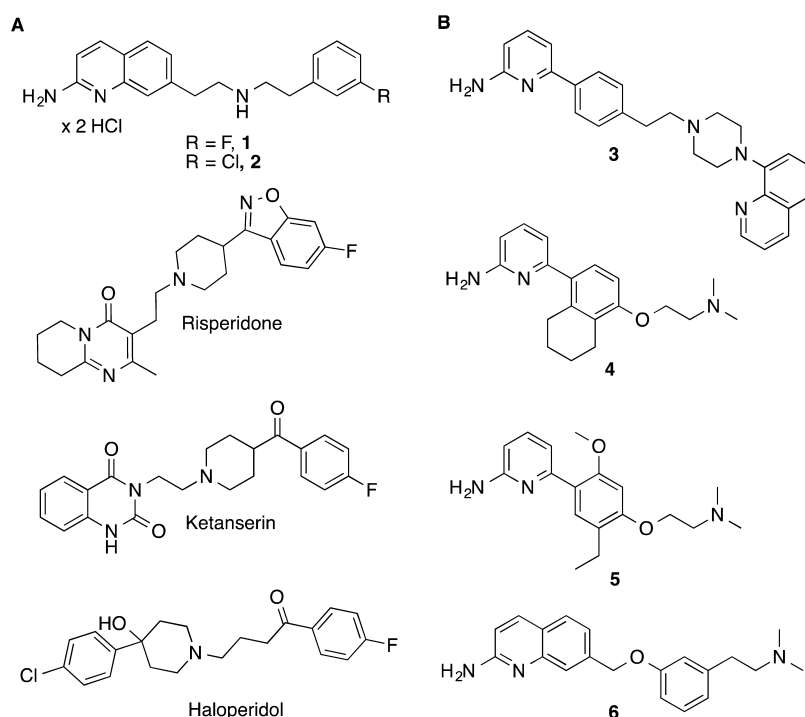
Figure 2. (A) Similarity of 1 and 2 to known "promiscuous" CNS binders; (B) truncation−inversion strategy (3 to 4 and 5) and design of compound 6.
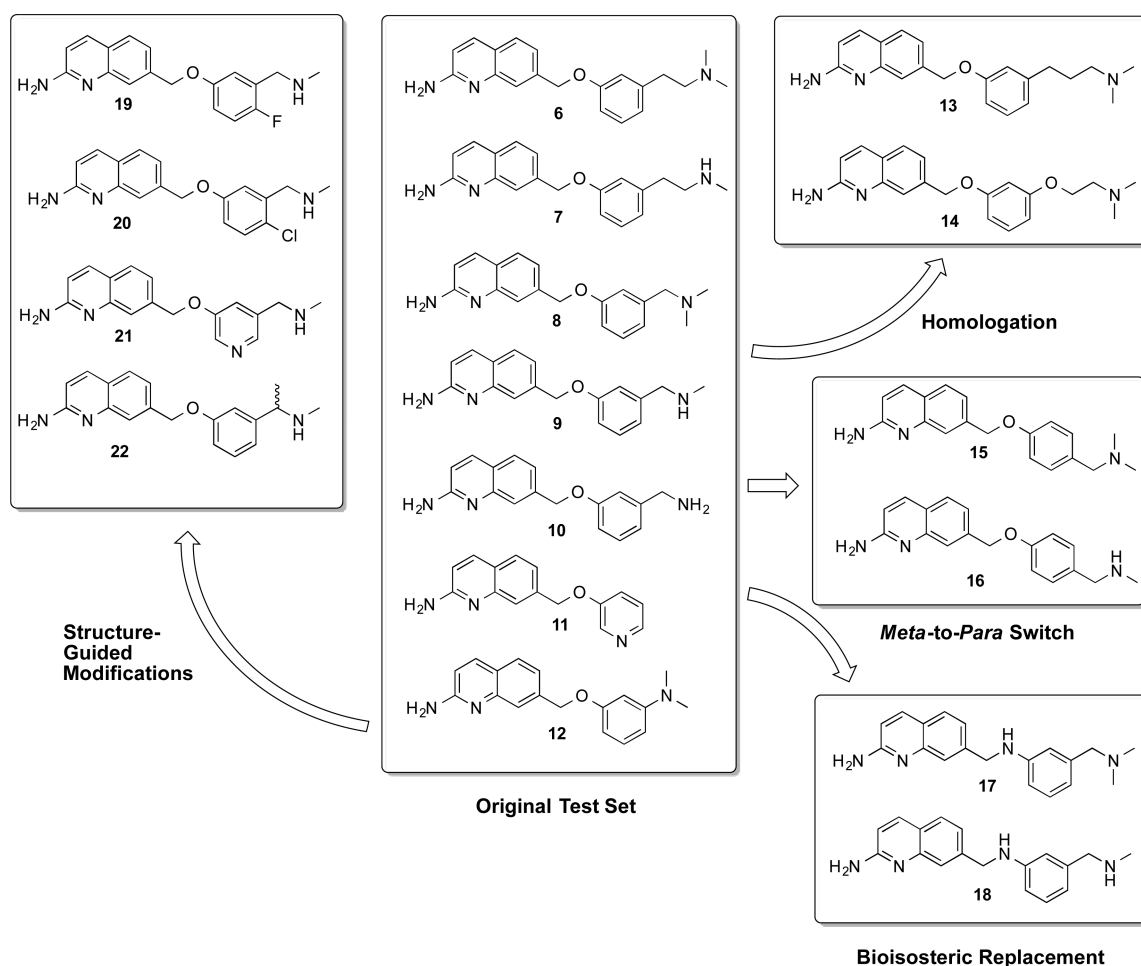
Figure 3. Molecules investigated in this study and overall design strategy.

molecule joined by a phenyl ether, the same as in **4** and **5**. We hypothesized that in addition to reducing off-target binding, this structural rearrangement could have additional benefits. First, the external amine of **6** could potentially form interactions in various spots peripheral to the nNOS active site such as Asp597, the H_4B site, or residues of the substrate access channel hydrophobic pocket, all of which have been shown to play significant roles in conferring potency or isoform selectivity.[26−28] Second, the predicted physicochemical properties of **6** are similar to those of **1** and **2** (CLogP: 2−4, <7 rotatable bonds, TPSA < 80 Å^2, and <4 hydrogen-bond donors), making it plausible that the cellular permeability of **1** and **2** could be preserved.

In addition to **6**, we designed and synthesized a small library of related compounds (**7−12**, Figure 3); all were assayed against purified rat nNOS, murine iNOS, and bovine eNOS. Encouraged by the potency and isoform selectivity of **8** and **9**, different modifications were performed to optimize the structure and examine the SAR. First, **13** and **14** were synthesized to investigate if longer tail lengths could provide additional or enhanced beneficial contacts with the enzyme. Second, although **8** and **9** have the amine-containing moiety located *meta* to the phenyl ether, *para*-substituted compounds **15** and **16** were also prepared to investigate the role that different ring substitution patterns may play. Third, we reasoned that bioisosteric replacement of the phenyl ether with an aniline (**17** and **18**) might introduce another contact in

the region near the heme propionates, resulting in greater affinity for nNOS.

Finally, we performed specific, structure-based optimizations to improve the potency and selectivity of lead **9**. X-ray crystallography indicated that the center aryl rings of **8** and **9** abut two residues, Tyr706 and Asn569. We hypothesized that introduction of halogens *para* to the phenyl ether linkage, as in **19** and **20**, could provide additional van der Waals interactions with Tyr706 or the surrounding hydrophobic structures. Likewise, by converting the phenyl ring to a pyridine (**21**), a hydrogen bond or polar contact could potentially form between the pyridine nitrogen and the side chain of Asn569. We also proposed that contacts might be made with other residues of the hydrophobic pocket (such as Met336 and Leu337) by placing a methyl group *alpha* to the exterior amine group of **9** (to yield **22**). All compounds were assayed against purified rat nNOS, and select compounds were assayed against eNOS, iNOS, and human nNOS, for cellular permeability in a Caco-2 model, and against a panel of CNS targets in the PDSP to assess their off-target binding.

Chemistry. Previously, 7-substituted-2-aminoquinolines were prepared via readily accessible chloroquinoline **23**[18,29] (Scheme 1) by performing a Kóródi amidation[30] to produce 2-acetamidoquinoline **25**. Unfortunately, this procedure gives irreproducible yields and is not readily amenable to scale-up. Smith et al.[31] reported the palladium-catalyzed amination of 2-chloroquinolines using LHMDS as both an ammonia surrogate

Scheme 1[a]
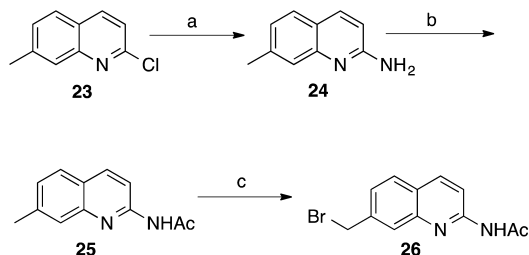
[a]Reagents and conditions: (a) LHMDS, Pd$_2$(dba)$_3$, DavePhos, THF/dioxane, 100 °C; (b) N-acetylimidazole, THF, reflux; (c) NBS, (PhCO$_2$)$_2$, benzene, reflux.

and base; applying this procedure to **23** afforded 2-amino-quinoline **24** in nearly quantitative yield on a multigram scale. Treatment with N-acetylimidazole in refluxing THF afforded **25**, and free-radical bromination (as previously reported) yielded versatile bromide **26**.

The phenol and aniline halves were then prepared. To prepare **6** (Scheme 2A), 3-methoxyphenethylamine (**27**) was dimethylated, and the O-methyl group of **28** was removed to yield phenol **29**. Monomethyl phenol **32** (needed for compound **7**) was prepared from 3-methoxyphenethyl bromide (**30**, Scheme 2B) and methylamine, followed by demethylation

Scheme 2[a]
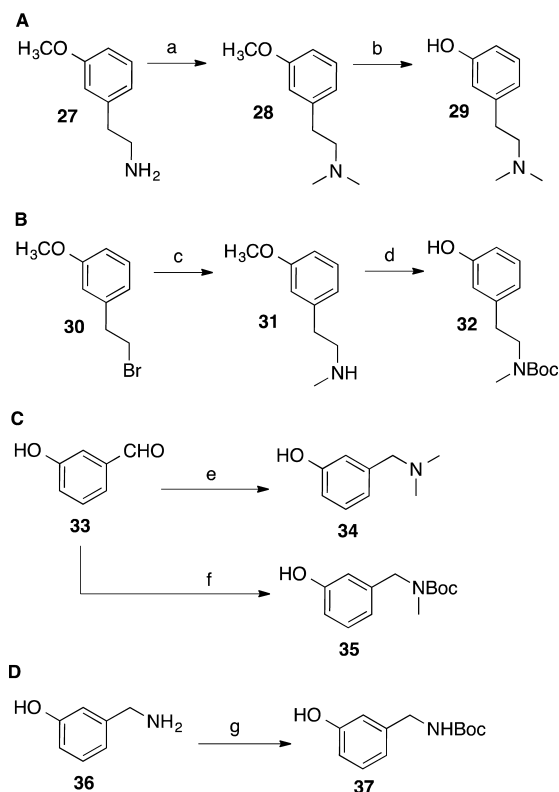
[a]Reagents and conditions: (a) formalin, formic acid, DMF, 60 °C−120 °C, 5 h; (b) 48% HBr, AcOH, reflux; (c) 40% MeNH$_2$ in H$_2$O, THF/H$_2$O, r.t.; (d) (i) 48% HBr, HOAc, reflux, (ii) Boc$_2$O, Et$_3$N, THF, r.t.; (e) (i) Me$_2$NH-HCl, Et$_3$N, CHCl$_3$/MeOH, Na$_2$SO$_4$ r.t., (ii) Na(OAc)$_3$BH, r.t., (f) (i) MeNH$_2$ in THF, cat. AcOH, CHCl$_3$/MeOH, Na$_2$SO$_4$, r.t.; (ii) NaBH$_4$ MeOH, 0 °C−r.t., (iii) Boc$_2$O, THF, r.t.; (g) Boc$_2$O, THF, 0 °C−r.t.

of **31** and immediate Boc-protection (to aid in purification and prevent later interference by the free secondary amine). For the benzylic amine of **8**, phenol **34** (Scheme 2C) was prepared by reductive amination of commercially available aldehyde **33** with N,N-dimethylamine. Similarly, exchanging N,N-dimethylamine for methylamine (needed for **9**) yielded an amine, which was protected as **35**. Phenol **37** (Scheme 2D) was prepared for the synthesis of **10** by Boc-protecting commercially available **36**.

The longer linker of **13**, via phenol **40**, was prepared by a Sonogashira coupling of 3-iodophenol **38** with N,N-dimethyl-propargylamine, followed by reduction of the triple bond of **39** to yield **40** (Scheme 3A). For compound **14**, **42** was prepared

Scheme 3[a]
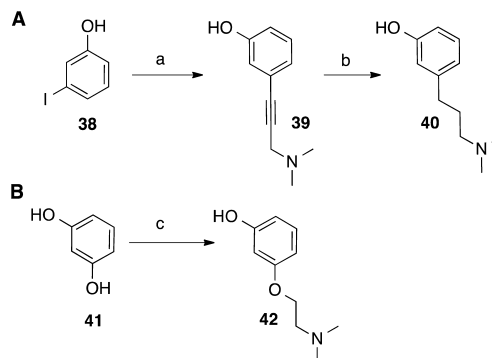
[a]Reagents and conditions: (a) N,N-dimethylpropargylamine, CuI (10 mol %), Pd(PPh$_3$)$_4$ (5 mol %), THF/Et$_3$N, r.t.; (b) H$_2$, Pd/C, MeOH, r.t.; (c) N,N-dimethylethanolamine, PPh$_3$, DEAD, THF, 0 °C, r.t.

by a Mitsunobu reaction between resorcinol **41** and N,N-dimethylethanolamine[32] (Scheme 3B). As performed for the meta-analogues, phenols **44** and **45** (for analogues **15** and **16**, respectively, Scheme 4) were prepared from 4-hydroxybenzal-dehyde (**43**) and either N,N-dimethylamine (for **44**) or methylamine (for **45**).
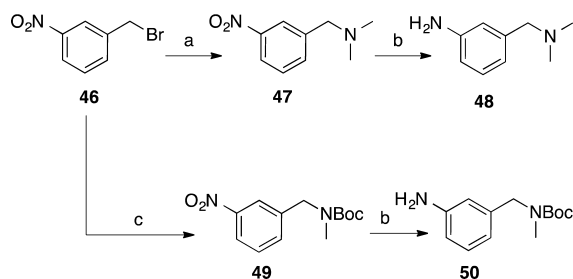
Scheme 4[a]
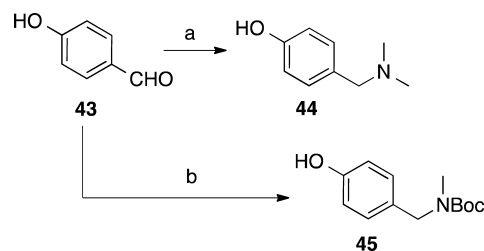
[a]Reagents and conditions: (a) (i) Me$_2$NH-HCl, Et$_3$N, Na$_2$SO$_4$, CHCl$_3$/MeOH, r.t.; (ii) Na(OAc)$_3$BH, r.t., (b) (i) MeNH$_2$ in THF, CHCl$_3$/MeOH, Na$_2$SO$_4$, AcOH, r.t.; (ii) NaBH$_4$, MeOH, 0 °C−r.t., (iii) Boc$_2$O, THF, r.t.

The anilines required for **17** and **18** were prepared from 3-nitrobenzyl bromide (**46**, Scheme 5) upon treatment with either dimethylamine (**47**) or methylamine (followed by Boc-protection to yield **49**). Reduction of the nitro group with Raney nickel afforded **48** (for **17**) and **50** (for **18**).

Finally, the substituted phenols (for **19**−**22**, Scheme 6A) could be prepared by employing the reductive amination/Boc protection protocol to commercially available aldehydes (**51**, **52**) or acetophenone **53**, to yield the protected amines **54**−**56**,

Scheme 5[a]

[a]Reagents and conditions: (a) Me$_2$NH-HCl, Et$_3$N, CH$_2$Cl$_2$/MeOH, r.t.; (b) H$_2$, Raney Ni, MeOH, r.t.; (c) (*ii*) MeNH$_2$ in THF, CH$_2$Cl$_2$, r.t., (*ii*) Boc$_2$O, CH$_2$Cl$_2$, r.t.

Scheme 6[a]
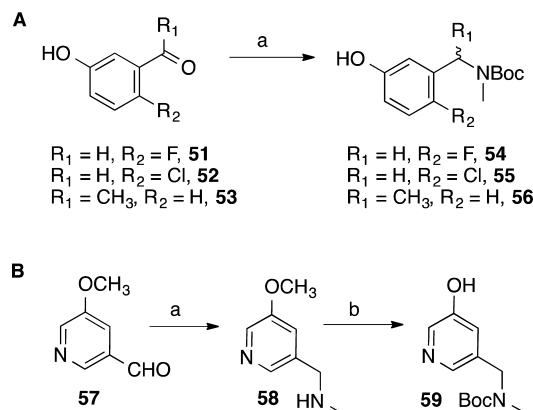
[a]Reagents and conditions: (a) (*i*) MeNH$_2$ in THF, cat. AcOH, CHCl$_3$/MeOH, Na$_2$SO$_4$, r.t., (*ii*) NaBH$_4$ MeOH, 0 °C–r.t., (*iii*) Boc$_2$O, THF, r.t.; (b) (*i*) HBr/H$_2$O, AcOH, 130 °C, (*ii*) Et$_3$N, Boc$_2$O, THF/MeOH, r.t.

respectively. Lastly, the pyridinol **59** (for **21**, Scheme 6B) was prepared by reductive amination of nicotinaldehyde **57** and cleavage of the methyl group of **58**; Boc-protection furnished **59**.

With the halves of the phenyl ether-substituted quinolines in hand, assembly of the final cores (Scheme 7) was completed by first treating the desired phenol [**29**, **32**, **34**, **35**, **37**, **40**, **42**, **44**, **45**, **54**−**56**, **59**, or commercially available 3-hydroxypyridine or 3-(*N*,*N*-dimethylamino)phenol (for compounds **11** and **12**, respectively)] with sodium hydride in DMF at 0 °C. A solution of **26** was then added; the reaction was typically complete within 1 h. Yields were good but were lower for the tertiary amines because of partial solubility in the aqueous DMF solutions produced in the workup. The intermediate acetamides (**60**−**74**) were not characterized and were deprotected immediately after purification: the acetyl group was first removed by K$_2$CO$_3$ in refluxing methanol, and after isolation, the free aminoquinolines were treated with methanolic HCl in ether to produce water-soluble hydrochloride salts. Compounds without a Boc group were isolated after 5−15 min; those with a Boc group were stirred overnight for deprotection. In the case of **72**, HCl induced unfavorable side reactions, so TFA was used instead.

The microwave alkylation procedure of Romero et al.[33] was employed to synthesize aniline **18** (Scheme 7). Compound **26**, excess **50**, and catalytic potassium iodide were heated in acetonitrile under microwave irradiation to furnish intermediate

75, which was deprotected as described above. Unfortunately, because of its nucleophilic amine, **48** only produced water-soluble quaternization products upon reaction with **26**. It was proposed that the two halves of *N*-linked compound **17** could be joined via reductive amination, beginning with the quinolinecarboxaldehyde **81**. After many unsuccessful attempts to prepare **81** from **25** and **26**, **81** was prepared in five steps[34] (Scheme 8), starting with a Wittig cyanovinylation of commercially available aldehyde **76**; the desired *trans*-isomer **77** was obtained in good yield. Iron-catalyzed reductive cyclization yielded aminoquinoline **78**, which was acetylated in good yield using *N*-acetylimidazole. Ester **79** was reduced to alcohol **80**, and oxidation to **81** was performed using Dess-Martin periodinane. An indirect reductive amination with **48** was effective at elevated temperatures, and the crude acetamide was deprotected to yield **18**.
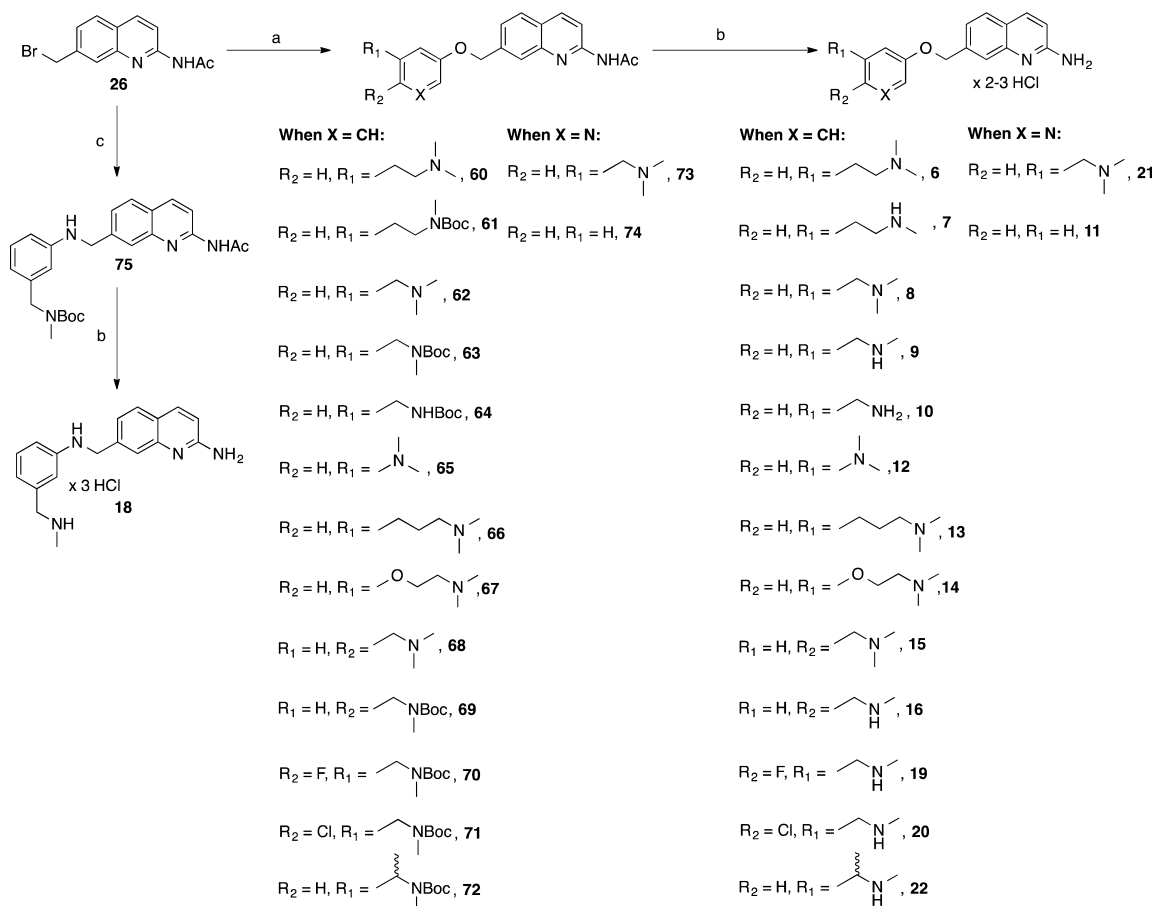
■ RESULTS AND DISCUSSION

Compounds **6**−**22** were first assayed against purified rat nNOS, murine macrophage iNOS, and bovine eNOS using the hemoglobin capture assay.[35,36] These species are used because (a) it is easiest to purify and readily obtain crystallographic data with these isozymes, and (b) there is a large active-site homology between mammalian species and therefore, while not 100% accurate, an adequate approximation of isoform selectivity can be obtained. Table 1 summarizes the apparent K_i values and isoform selectivity values for **6**−**22**; for the sake of comparison, values for **1** and **2** are included.

The first series of compounds, **6**−**12**, is less potent than **1** or **2**. At first glance, it appears that compounds with a basic amino group (**6**−**10**) are more potent against nNOS than those with less basic groups such as pyridine (**11**) and *N*,*N*-dimethylaniline, which rendered compound **12** essentially inactive. The positioning of the tail amino group plays a role in enzyme−inhibitor interactions. The crystal structures of nNOS-**6** and nNOS-**7** are compared side by side in Figure 4. The strong 2-aminoquinoline-Glu592 (arginine mimic) interaction characteristic of this class is well supported by the strong electron density. In contrast, the central aryl ring and the tail regions show rather weak density, indicative of disordering. The methylamine of **7** reaches the H$_4$B site because the tail is long enough to displace the water molecule normally present in this site, and H-bond either with H$_4$B or with the nearby heme propionate (Figure 4B). This interaction pushes the central aryl ring into nonbonded contact with the Tyr706 side chain. However, the tertiary amino group of **6** does not interact with H$_4$B or heme, but hangs adjacent to Met336 because the central aryl ring presses against the heme propionate (Figure 4A). The lack of both the H$_4$B site and Tyr706 contacts likely explains why **6** is less potent than **7**.

When the tail is one methylene shorter, (**8** and **9** vs **6** and **7**, respectively) the potency is also increased. As shown in Figure 5, the tertiary amino group of **8** can form an H-bond with Asn569, while the secondary amino group of **9** is involved in a water-mediated H-bonding network with H$_4$B and heme. The phenyl ring of **9** forms a pi-stacking interaction with Tyr706 (these rings are >4 Å apart in the nNOS-**8** structure). These same interactions are observed in the nNOS-**10** structure, which has a primary amino group, (see Supporting Information, Figure S1).

Two trends are clear. First, potency is increased slightly upon removal of one methyl group from the tertiary amines; **9** and **10** are more potent than **8**, and **7** is more potent than **6**. The

Scheme 7[a]

Scheme 8[a]
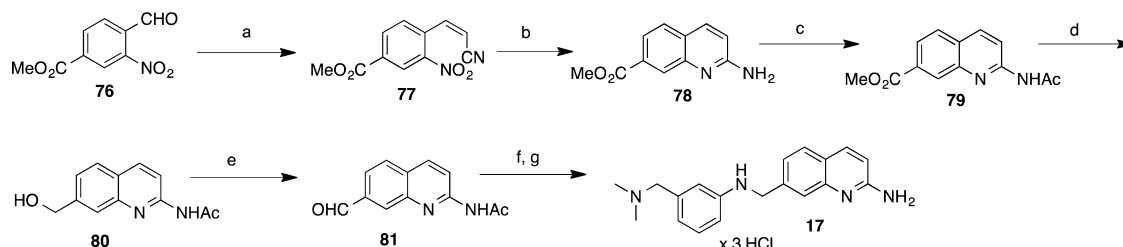
protonated secondary amino group bears two hydrogens and is a stronger H-bond donor than the tertiary amino group, as demonstrated by **7** and **9**. Second, the longer chains of **6** and **7** show higher flexibility (structure disordering) in the phenyl ether and tail region when compared to that of **8** and **9** and thus could result in weaker or partial interactions as a result of entropy, leading to lower potency than that of **8** and **9**. Interactions with Asn569 or the H$_4$B site are crucial for the activity of these compounds; the short amino group of **12** is incapable of forming these interactions, and this could be why **12** has little activity.

Interestingly, the n/e selectivity for **8** and **9** is similar to that observed for **1** or **2**. It is known that contact between the halophenyl rings of **1** and **2** and the hydrophobic pocket residues Tyr706, Leu337, and Met336 improves potency and n/e selectivity.[18] What is responsible for the n/e selectivity for these compounds lacking obvious hydrophobic contact? X-ray crystallography indicates that in eNOS, a common binding mode is observed for most phenyl ether-linked aminoquinolines, characterized by an "upward" position of the ether bond, where the phenyl ring sits perpendicular to the plane of the aminoquinoline. In the eNOS-**9** structure (Figure 6A), the

Table 1. Inhibition of NOS Enzymes by Phenyl Ether and Aniline Compounds

| compd | K_i (μM)[a] | | | selectivity | |
	nNOS	iNOS	eNOS	n/i	n/e
1	0.049	44.0	11.16	899	228
2	0.066	28.4	7.24	431	110
6	0.468	150	17.7	320	38
7	0.332	43.6	15.1	131	45
8	0.179	60.2	18.0	338	101
9	0.142	33.2	25.3	237	178
10	0.160	33.6	12.9	210	80
11	0.712	NT	NT	ND	ND
12	>5.75	NT	NT	ND	ND
13	0.652	NT	NT	NT	ND
14	0.475	178	31	379	44
15	0.283	117	31.4	413	111
16	0.332	48.7	NT	147	ND
17	0.375	33.2	11.5	89	31
18	0.569	NT	NT	ND	ND
19	0.147	11.4	NT	78	ND
20	0.058	27.7	12.5	478	216
21	0.043	13.5	3.31	313	77[b]
22	0.360	67.1	NT	186	ND

[a]The compounds were assayed for in vitro inhibition against three purified NOS isoforms: rat nNOS, bovine eNOS, and murine iNOS, using known literature methods (see Experimental Section for details), and K_i values are calculated directly from IC$_{50}$ values. IC$_{50}$ values are the average of at least two replicates from 7 to 9 data points; all experimental standard error values are less than 12%, [b]except for the eNOS value for **21**, which is 19%. All correlation coefficients are good ($R^2 > 0.82$). Selectivity values are ratios of respective K_i values. NT = not tested; ND = not determined.

perpendicular orientation of the phenyl ring breaks the pi-stacking interactions with Tyr706 (distance >6 Å), and the phenyl ring and methylamine portion can be modeled in alternate conformations where the amine can either face toward or away from the H$_4$B site. Similar upward phenyl ring positions are also observed for **7** and **8** bound to eNOS (see Figure S2), indicating that this position occurs regardless of tail length or amine alkylation pattern.

While the perpendicular orientations found in these eNOS structures would diminish many of the interactions that confer binding to nNOS (and thus result in the observed n/e selectivity), it was unclear what structural difference between

nNOS and eNOS resulted in these binding modes. Further complicating the interpretation of the eNOS structural data is the presence of both glycerol and acetate (crystallization buffer components) in all of the eNOS structures. While the glycerol is located peripherally relative to the inhibitor, the acetate (found in eNOS because of the alternate rotamer assumed by Arg252) abuts the perpendicular phenyl rings of the inhibitors and in several cases results in clearer electron density in the crystal structures, suggesting that the perpendicular binding modes may be stabilized by nonbonded contacts with the acetate and are thus likely a crystallographic artifact. By removing acetate from the cryo-soaking buffer, we were able to confirm that acetate is, indeed, the reason for some of these inhibitors to adopt a different binding mode in eNOS. This will be considered in more detail when the structures of **20** bound to eNOS and nNOS are discussed below.

To confirm this hypothesis further, the rat nNOS double mutant D597N/M336V was employed, where Asp597 and Met336 are mutated to, respectively, the corresponding asparagine and valine found in bovine eNOS. This enzyme has previously been used as an eNOS "surrogate" to elucidate the effects that amino acid differences have on inhibitor binding.[37,38] While the active-site sequence resembles eNOS, the overall local environment and domain architecture still resemble wild-type rat nNOS; Arg481 (the equivalent of Arg252) is retained in the WT nNOS rotameric state, and acetate no longer binds. In the nNOS-D597N/M336V-**9**-structure (Figure 6B) the phenyl ether portion of **9** reverts to the coplanar binding mode observed in WT rat nNOS and *not* the perpendicular mode observed in the eNOS-**9** structure, indicating that the upward position of the phenyl ring is likely stabilized or induced by the acetate. Nonetheless, a difference in the positioning of the methylamine tail in the nNOS-D597N/M336V-**9** structure (Figure 6B) could explain the observed selectivity for nNOS over eNOS. In the WT nNOS structure, the methylamine tail rotates away from bulky Met336, and the amino group faces toward the bridging water in the H$_4$B site (Figure 5B). In the double mutant structure, the smaller Val336 (analogous to eNOS' Val106) allows for the amine to instead face toward the hydrophobic pocket, breaking the H$_4$B site interaction. This is not the first reported case where subtle differences in Met/Val contacts have led to large effects on n/e selectivity[18,39] and also serves as a cautionary note against over-reliance on X-ray structures in interpretation of SAR data. As no acetate is used in the eNOS purification or assay, the
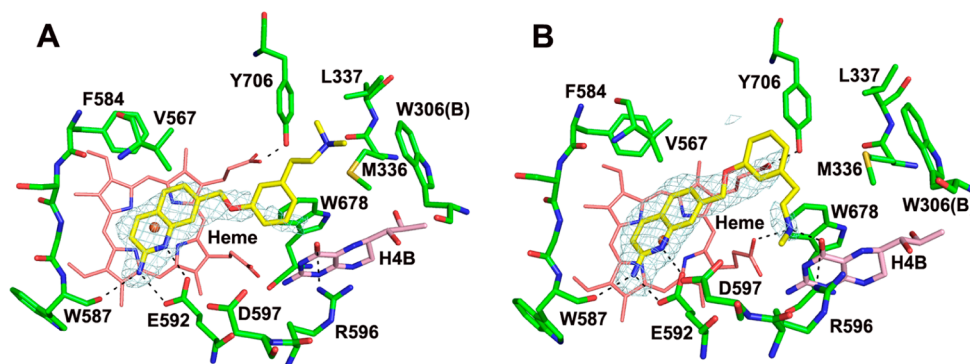
Figure 4. Active site structure of **6** (A) or **7** (B) bound to rat nNOS. The omit $F_o - F_c$ density map for the inhibitor is shown at the 2.5 σ contour level. The tail of **6** shows weaker density indicative of disordering. The alkylamine of **7** displaces a water molecule, thus making H-bonds with both H$_4$B and the heme. Major hydrogen bonds are shown as dashed lines. Figures prepared using PyMol (www.pymol.org).
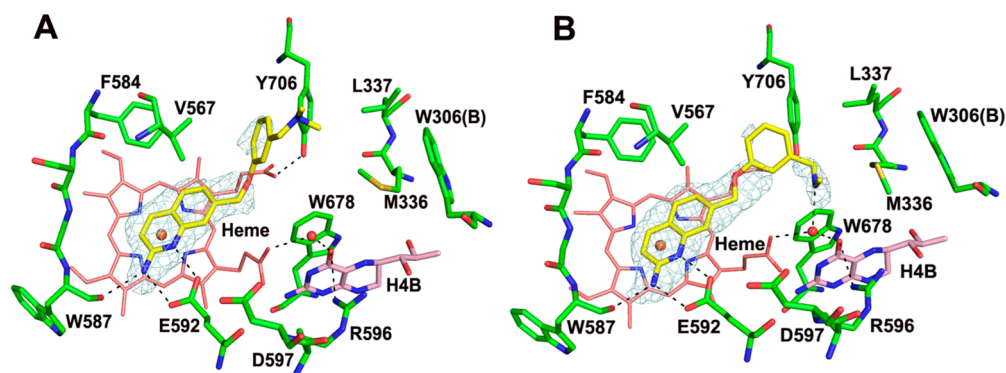
Figure 5. Active site structure of **8** (A) or **9** (B) bound to rat nNOS. The omit $F_o - F_c$ density map for the inhibitor is shown at the 2.5 σ contour level. The tail of **8** shows weaker density, indicative of disordering. The dimethylamine of **9** makes a H-bond with the water molecule bridging both H4B and heme. Major hydrogen bonds are shown as dashed lines.
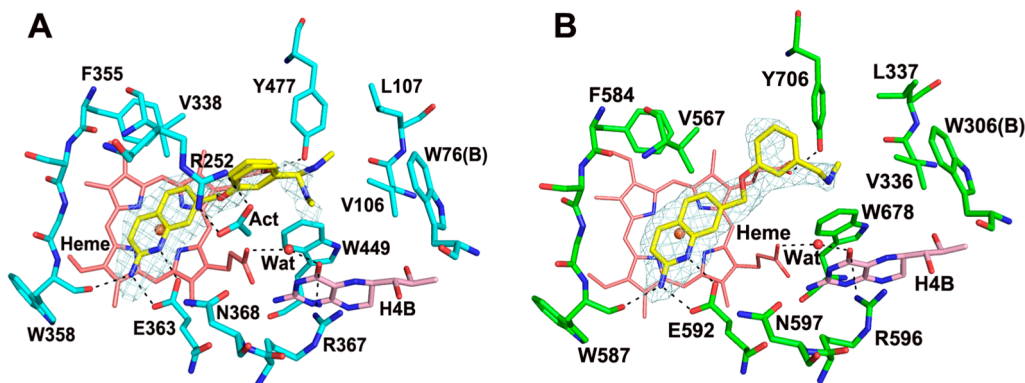
Figure 6. Active site structure of **9** bound to bovine eNOS (A) and rat nNOS D597N/M336V double mutant (B). The omit $F_o - F_c$ density map for the inhibitor is shown at the 2.5 σ contour level. An acetate ion (Act) is stabilized by Arg252 in eNOS, which in turn makes contacts with the phenyl ring of **9**. Major hydrogen bonds are shown as dashed lines.
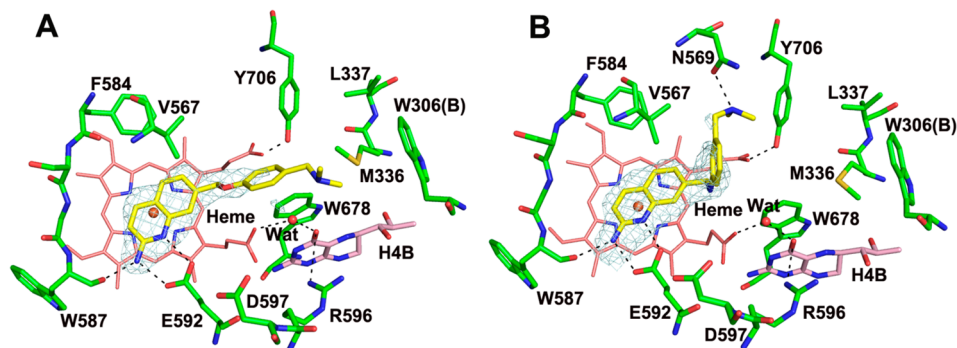

Figure 7. Active site structure of **15** (A) or **17** (B) bound to rat nNOS. The omit $F_o - F_c$ density map for the inhibitor is shown at the 2.5 σ contour level. Major hydrogen bonds are shown as dashed lines.

observed eNOS selectivity for **9** was assumed to result from actual structural changes by comparing WT nNOS-**9** and nNOS-D597N/M336V-**9** structures. Assaying **9** against nNOS-D597N/M336V yielded a K_i of 585 nM. This value is 4-fold higher than the WT nNOS K_i, indicating that the Met-to-Val switch indeed disfavors binding to the double mutant. This value is also considerably lower than the eNOS K_i value (25.3 μM), demonstrating that different amino acids are also not the full determinant of selectivity; subtle differences in sterics, electronics, or the local active site environment could also be responsible.

Although **6** and **7** are less potent than the shorter compounds (**8**−**10**), we reasoned that elongation of the alkyl chain by one methylene unit (to phenylpropyl, such as in **13** and **14**) might either force the N-methyl groups toward the nNOS-specific hydrophobic pocket or place the basic amine near Asp597. Asn368 replaces Asp597 in eNOS (vide supra), and electrostatic or water-mediated contact with the latter residue has been previously implicated in high n/e selectivity.[26,40] Disappointingly, this modification was ineffective: **13** and **14** are less potent than **6**. Loss of activity upon extensive homologation was seen previously for 2-aminoquinoline compounds,[18] hypothesized to result from sterically disfavored, suboptimal, or partial interactions, or internal torsional strain.

H
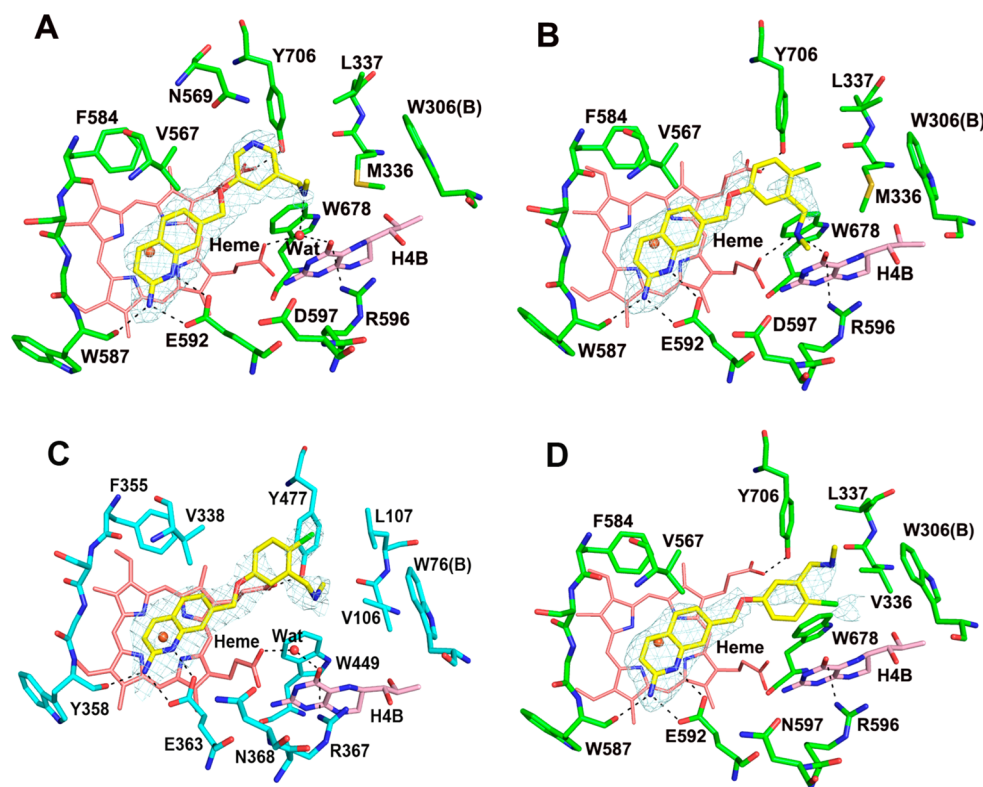
Figure 8. Active site structure of **21** (A) or **20** (B) bound to rat nNOS, **20** bound to acetate-free eNOS (C), or **20** bound to rat nNOS D597N/M336V double mutant (D). The omit $F_o - F_c$ density map for the inhibitor is shown at the 2.5 σ contour level. The dimethylamine of **20** displaces the water molecule bridging H_4B and heme in the WT nNOS but not in the acetate-free eNOS or the nNOS double mutant structures. Major hydrogen bonds are shown as dashed lines.

We also synthesized *para*-substituted analogues **15** and **16** to investigate whether different ring substitution could improve potency or selectivity. Compound **15** has lower potency than *meta*-substituted analogue **9** (K_i 283 nM vs 142 nM), and desmethyl compound **16** is slightly less potent than **15**, indicating that the binding mode of these compounds must be different from the *meta*-substituted analogues. The nNOS-**15** crystal structure (Figure 7A) indicates that the phenyl ring of **15** is oriented quite differently from that of **9**. The alkylamine tail of **15**, as a *para*-substituent, extends out farther with high flexibility. The methyl group makes possible contact with Met336, but the amine loses its effective H-bond interaction with the H_4B site water. The flexible nature of the tail may allow it to make both the hydrophobic pocket and H_4B site contacts transiently.

We also employed the secondary aniline (**17** and **18**) as a bioisosteric replacement for the ether oxygen. Crystal structures of the phenyl ether-linked compounds indicated a possible placement for the NH group between the heme propionates, where it could make another electrostatic or H-bonding interaction. Surprisingly, the potency for **17** was lower than that of **8**, and the loss of additional potency upon demethylation (to **18**) indicated that **17** and **18** do not bind like **8** and **9**. The nNOS-**17** structure (Figure 7B) reveals instead that the aminoquinoline and central aryl rings sit ~120° relative to each other in a "butterfly" position, reflecting the geometry required for the aniline nitrogen to interact with the nearby heme propionate. As a result, the aryl ring moves upward, and the dimethylamine H-bonds to Asn569. It is not evident from this structure as to why **17** should be a worse nNOS inhibitor than **8** (or why demethylation should further

attenuate the activity), but both steric crowding around the Asn569-dimethylamine area (highly disordered in the crystal structure) and the lack of the inhibitor-Tyr706 *pi*-stacking interaction observed in **8** and **9** could play a role. Additionally, the eNOS-**17** structure (see Figure S3) reveals a nearly identical binding mode to that assumed in the nNOS-**17** structure, which could be consistent with the low selectivity of **17**.

While the addition of a fluorine or α-methyl group to **9** (to give **19** or **22**, respectively) was neutral (**19**) or a deleterious (**22**) modification with regard to both potency and selectivity (relative to **9**, and thus were not investigated further or examined crystallographically), the replacement of the phenyl ring of **9** with pyridyl (**21**) resulted in a substantial increase in potency (K_i 142 nM to 43 nM; more potent than **1** and **2**). The nNOS-**9** structure indicated the potential for the ring nitrogen to make an additional contact with Asn569, a prediction proven correct by the nNOS-**21** structure (Figure 8A). Compound **21** assumes a well-defined, **9**-like binding mode, where the external amine binds the H_4B-site water and the pyridine ring simultaneously forms an edge-to-face *pi*-stacking interaction with Tyr706 and a polar contact with Asn569 (although at 3.7 Å, it is likely too far for a true H-bond). The high potency of **21** also highlights the absolute necessity of the external polar amine; compound **11**, the unsubstituted 3-pyridine, binds nearly 17-fold weaker to nNOS than **21**. While potent, **21** does not possess improved n/e selectivity relative to that of **9**: this asparagine residue is conserved across all NOS isoforms, and interaction with the pyridine likely nonspecifically increases binding affinity to other isoforms, as manifested by the decreased K_i values for eNOS and iNOS as well.

In contrast to *para*-fluoro compound **19**, the *para*-chloro analogue **20** is much more potent than compound **9**, with high isoform selectivity comparable to that of **1** and **2**. The nNOS-**20** structure (Figure 8B) shows that the phenyl ring is flexible, having two possible orientations in the two nNOS monomers, where the amine can either displace the H_4B-site water or point toward the hydrophobic pocket by rotation of the phenyl ring, while the chlorine can make van der Waals contacts with Met336. The fluorine atom of **19** could be too small to make the latter contact, whereas the α-methyl group of **22** may be sterically disfavored in this region.

The eNOS-**20** crystal structure (see Figure S4) also displays the "upward" binding mode and the stabilizing acetate ion. However, if acetate is removed from the cryo-soaking buffer, the phenyl ring of **20** no longer adopts the upward orientation (Figure 8C) but points toward the pocket bound by Val106, Leu107, and Tyr477, similar to the binding mode observed in the rat nNOS double mutant D597N/M336V-**20** structure (Figure 8D). In addition, the positions of the phenyl ring and its two substituents (chlorine and methylamine) are better resolved than in the double mutant nNOS structure. The methylamine tail contacts Val106 but does not H-bond with the H_4B or heme propionate A as observed in the wild type nNOS structure (Figure 8B). The chlorine makes no contact with Val106. As this binding mode is quite similar to that found in the double mutant structure (Figure 8D), we can confirm that acetate strongly influences the binding mode of inhibitors in eNOS structures and that the nNOS double mutant is indeed a good mimic of eNOS. In the nNOS double mutant-**20** structure (Figure 8D), the Met-to-Val switch causes a significant change in binding mode: the phenyl ring has a single orientation rather than the two different ones observed in WT nNOS. The amine-H_4B site interaction is broken; instead, the methylamine tail fits in the hydrophobic pocket, larger because of the smaller Val336 residue. In addition, there is a lack of van der Waals contact between **20**'s chlorine atom and Val336. Assaying **20** against nNOS D597N/M336V gave a K_i value (863 nM) that is in between that of the WT nNOS (58 nM) and eNOS (12.5 μM) K_i values, indicating, like for **9**, that differences in amino acid sequences (such as Met to Val) do not fully account for the observed selectivity. Nonetheless, the double mutant nNOS/wild-type nNOS selectivity ratio (15) is higher than **9**'s (4) showing, as the crystal structure does, that the inhibitor-Met336 contact plays a greater role in n/e selectivity for **20** than it does for **9**.

In addition to the good n/e selectivity, the majority of the phenyl ether compounds are also poor iNOS inhibitors (20–150 μM). We had previously reported this incompatibility between iNOS and 2-aminoquinolines.[17] The high n/i selectivity was attributed in part to the mismatch between the smaller and more rigid heme-binding pocket of iNOS[41] and the bulky aminoquinoline, and in part to hydrophobic pocket contacts (as murine iNOS contains a polar residue, Asn115, in place of Leu337 of rat nNOS). Indeed, a bulky and hydrophobic group, such as chlorophenyl, may clash in the region of Asn115 and possibly lead to the high n/i selectivity observed for **20**.

Several compounds of interest (**6**, **8**, **9**, **15**, **17**, **20**, and **21**) were also assayed against purified human nNOS (Table 2). The human nNOS active site differs from rat nNOS by one residue: Leu337 is replaced by His342.[42,43] The peripheral pocket of human nNOS, therefore, prefers binding smaller and more hydrophilic fragments, as evident from the high rat nNOS/

**Table 2. Inhibition of Rat and Human nNOS by Select Compounds[a]**

compd	K_i (μM)[a]		selectivity (rat/human)
	rat nNOS	human nNOS	
1	0.049	0.318	6.5
2	0.066	0.440	6.7
6	0.468	1.86	4.0
8	0.179	0.855	4.8
9	0.142	0.911	6.4
15	0.283	1.08	3.8
17	0.375	0.657	1.8
20	0.058	0.295	5.1
21	0.043	0.507	11.8

[a]The compounds were assayed for in vitro inhibition against human nNOS using known literature methods (see Experimental Section for details), and K_i values are calculated directly from IC_{50} values. IC_{50} values are the average of at least two replicates from 7 to 9 data points; all experimental standard error values are less than 12%, and all correlation coefficients are good ($R^2 > 0.87$). Selectivity values are ratios of respective K_i values; rat nNOS K_i values are from Table 1.

human nNOS selectivity for the hydrophobic-tailed compounds **1** and **2**. If the bound inhibitor cannot reach the Leu/His site, an identical binding mode should be found in both rat and human nNOS structures.[42] Aniline **17** is a typical example. In the human nNOS-**17** structure (see Figure S5), the "butterfly" binding mode is identical to that found in the rat nNOS-**17** structure, and the bound inhibitor is far from the Leu/His site. Therefore, there should be little selectivity (r/h = 1.8 only) between these two nNOS enzymes. Most of the ether-linked compounds are poor human nNOS inhibitors ($K_i = 1–2$ μM). The most potent human nNOS inhibitor, **20**, is still selective for rat nNOS over human nNOS, even though it is approximately as potent as **1**. The human nNOS-**20** structure (Figure 9A) shows a consistent phenyl ring orientation where the dimethylamine makes an H-bond with the H_4B site water; whereas in the rat nNOS-**20** structure (Figure 8B), the phenyl ring rotates and allows the dimethylamine to displace the H_4B site water molecule in one orientation but extends the amine to the hydrophobic pocket in the other orientation (not shown). Apparently, the bulkier His342 in human nNOS influences the phenyl position of **20** differently than Leu337 in rat nNOS.

Pyridine analogue **21** strongly prefers to bind to rat nNOS (r/h = 11.8), although the binding mode shows almost no difference in the two nNOS structures (Figure 9B for human). The only subtle difference observed in the structures is the side chain orientation of Tyr706 in rat compared to that of Tyr711 in human nNOS (because of the closer contacts from His342 in the human enzyme). A slight change in the edge-to-face *pi*-stacking interaction between the tyrosine and the inhibitor's pyridyl ring, however, would likely not fully account for the great difference in inhibitory potency.

Encouraged by the potency and selectivity of **20**, this compound was tested in a Caco-2 assay (Table 3), in which a compound's ability to cross a monolayer of cells (resembling the intestinal lumen) is measured. This assay can be used to approximate the permeability of the gut epithelium, and, to a lesser extent, the BBB.[44,45] Compound **1**, an orally bioavailable, brain-penetrant nNOS inhibitor, has good membrane permeability in the apical to basolateral (A → B) direction (a mean P_{app} of 16.9×10^{-6} cm s^{-1}), high compound recovery values, and a low efflux ratio [ratio of membrane permeability (A → B)
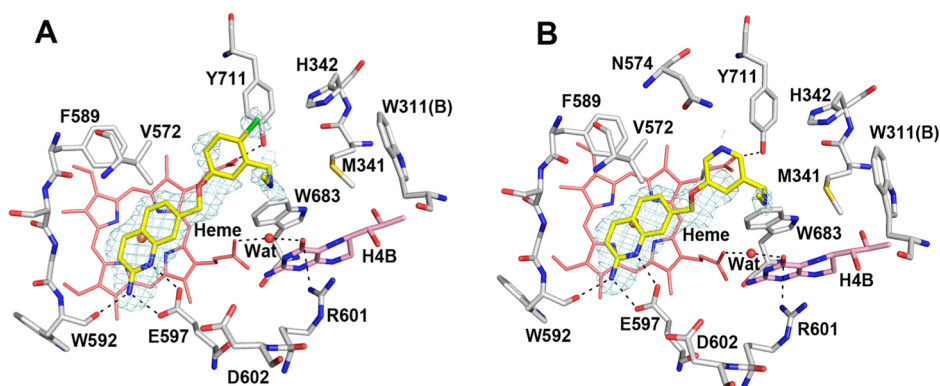
Figure 9. Active site structure of **20** (A) or **21** (B) bound to human nNOS. The omit $F_o - F_c$ density map for the inhibitor is shown at the 2.5 σ contour level. Major hydrogen bonds are shown as dashed lines.

Table 3. Caco-2 Permeability Summary for Select Compounds[a]

	apparent permeability (P_{app}, 10^{-6} cm s^{-1})[b]			recovery	
compd	mean A → B	mean B → A	efflux ratio	A → B	B → A
20	2.3	12.6	5.5	37%	79%
warfarin[c]	21.1	8.2	0.39		
ranitidine[d]	0.084	1.9	22.6		
talinolol[e]	0.061	7.6	125		

[a]All assays were performed over 2 h at a concentration of 10 μM. See Experimental Section for details. [b]Apparent permeability value. [c]High permeability control. [d]Low permeability control. [e]High efflux control.

to efflux (B → A), < 3 is considered favorable]. Unfortunately, compound **20** is less cell-penetrant, has a slightly higher efflux ratio than **1**, and has a lower A → B recovery value, potentially indicative of poor solubility or metabolic lability in these cells. Nonetheless, although suboptimal, some permeability is retained despite the drastic structural rearrangement.

Finally, **20** was screened by the PDSP.[19] In this assay, compounds are assayed against a panel of 45 pharmacologically relevant CNS targets via radioligand binding assays. We have classified off-target binding (Table 4) into four categories:

Table 4. PDSP Binding Summary for Select Compounds[a]

compd	concerning	moderate	weak	insignificant	total
2	8	7	22	8	45
20	3	3	17	22	45

[a]Off-target binding is classified into four categories: concerning ($K_i <$ 100 nM, or $\sim$2× nNOS K_i value), moderate (100−300 nM, $\sim$ 2−5× nNOS K_i value), weak (>300 nM, or > $\sim$5× nNOS K_i value, typically $\sim$1 μM), and insignificant (<50% bound at 10 μM), for a total of 45 receptors as assayed by the PDSP's "comprehensive screen". See ref 18. The three concerning targets for compound **20** are the alpha-2C adrenergic receptor, histamine H2 receptor, and the serotonin transporter (SERT).

concerning ($K_i <$ 100 nM, or < $\sim$2× nNOS K_i value), moderate (100−300 nM, $\sim$2−5× nNOS K_i value), weak (>300 nM, or > $\sim$5× nNOS K_i value, typically $\sim$1 μM), and insignificant (<50% at 10 μM). For compound **2**, a promiscuous scaffold with low therapeutic index, binding was considered concerning or moderate at 15/45 targets (mostly serotonin and histamine receptors), with 22/45 targets classified as weak, and 8/45 as insignificant. For compound **20**, the concerning/moderate

binding fraction has decreased to 6 targets, and the insignificant binding fraction has increased considerably, from 8/45 to 22/45, with the majority of the decrease coming from serotonin receptors. These results indicate that truncation and structural rearrangement, as observed for **4** and **5**, are effective at reducing off-target CNS binding and could potentially translate to improved safety in vivo, making the phenyl ether-linked core an exciting scaffold for further optimization.

CONCLUSIONS

To summarize, we have developed a novel series of 2-aminoquinoline-based nNOS inhibitors, using the rationale that this particular "rearranged" scaffold could maintain or enhance the potency and isoform selectivity of our previous leads (**1** and **2**) while diminishing the off-target binding of these compounds. Assaying this new generation of inhibitors (containing an exterior polar amine and an interior hydrophobic portion linked to the aminoquinoline via a phenyl ether or aniline) against purified NOS enzymes indicated that **9**, while having lower potency than **1** or **2**, maintained the triple-digit isoform selectivity of the leads. X-ray crystallography (using rat nNOS and a rat nNOS double mutant) indicated that the n/e selectivity might arise from enhanced hydrophobic contacts between the tail of the inhibitor and the nNOS-specific hydrophobic pocket. Elongating the chain between the aryl ring and the amine, changing the ring substitution pattern, and replacing the phenyl ether linkage with an aniline failed to improve **9**'s potency and selectivity, but one compound (**20**), chlorinated on the central aryl ring, was found to be a potent and selective inhibitor of both rat and human nNOS. Although lower than compound **1**, **20** still displayed some cellular permeability in a Caco-2 assay despite the significant structural rearrangement. Most promisingly, when assayed against a panel of 45 relevant CNS targets and receptors in the PDSP, **20** showed diminished off-target interactions relative to those of **2** (a promiscuous binder) indicating that potent and selective compounds based on the inverted phenyl ether core may have the potential for improved safety in vivo.

EXPERIMENTAL SECTION

General Procedures. Anhydrous solvents (THF, CH$_2$Cl$_2$, MeOH, and DMF) were distilled prior to use. The remaining solvents, reactants, and reagents were purchased from commercial vendors and were used without further purification. Methanolic HCl (3 M, for ammonium salt formation and Boc-deprotection) was prepared fresh by the reaction of acetyl chloride and anhydrous MeOH at 0 °C. Melting points were determined in capillary tubes using a Buchi

melting point B-540 apparatus and are uncorrected. ^{1}H NMR spectra were recorded at 500 MHz, using a Bruker Avance III 500 (direct cryoprobe), and ^{13}C NMR spectra were obtained at 126 MHz using the same instrument. Low-resolution ESIMS was performed using a Bruker AmaZon SL Ion Trap mass spectrometer system. High-resolution mass spectral data were obtained at the Integrated Molecular Structure Education and Research Center (Northwestern University) on an Agilent 6210A TOF mass spectrometer in positive ion mode using electrospray ionization with an Agilent G1312A HPLC pump and an Agilent G1367B autoinjector. Data were processed using MassHunter software, version B.04.00. Flash column chromatography was performed using an Agilent 971-FP automated flash purification system with a Varian column station and SiliCycle cartridges (12–80 g). Analytical HPLC was performed using an Agilent Infinity 1260 HPLC system and injection volumes of 5–10 μL. A Phenomenex Luna 5 μm C-8(2) 100 Å column, 50 × 4.60 mm, was used for all HPLC experiments, using a 10 min gradient of 95% H_2O/5% acetonitrile + 0.05% TFA to 95% acetonitrile/5% H_2O + 0.05% TFA, at 1.5 mL/min. The purity of all final target compounds was found to be ≥95% by HPLC. Preparative HPLC was performed at the Northwestern University Center for Molecular Innovation and Drug Discovery ChemCore laboratory, using an Agilent 1200 Series HPLC and Agilent 6120 Quadrupole Mass Spectrometer (API-MS mode) and 150 × 21.2 mm preparative HPLC columns (described under subheadings for individual compounds). Microwave chemistry was performed using a Biotage Initiator Sixty research microwave in Biotage vials. Analytical thin-layer chromatography was performed on Silicycle extra hard 250 μm TLC plates. Compounds were visualized with short-wavelength UV light and with ninhydrin, $FeCl_3$, and $KMnO_4$ stain, where relevant. Compounds **23**,[18] **26**,[31,46] **31**,[47] **37**,[48] and **42**[32] were prepared by known literature procedures, and their spectral data are consistent with those data reported for them. The preparations of phenols, anilines, and precursors **28–59** are discussed in the Supporting Information.

2-Amino-7-methylquinoline (24). Compound **23** (1.00 g, 5.63 mmol), DavePhos (0.051 g, 2 mol %), and $Pd_2(dba)_3$ (0.051 g, ~1 mol %) in a sealed tube or Biotage 20 mL microwave vial were diluted with anhydrous dioxane (6 mL), and LHMDS (1 M in THF, 12 mL, 12 mmol) was added slowly. The reaction was purged with argon for 5 min, sealed, and heated to 100 °C for 20 h. The mixture was cooled and poured into aqueous HCl (1 M, 20 mL) and stirred for 10 min before EtOAc (20 mL) was added. The layers were separated, and the aqueous layer was extracted with 1 M HCl (3 × 50 mL); the aqueous phase was washed repeatedly with EtOAc (3 × 30 mL), and the combined organic phase was discarded. The aqueous phase was basified to pH 9 with NaOH and extracted with EtOAc (2 × 150 mL). The organic phase was washed with sat. aq. NaCl (100 mL), dried, and concentrated to yield the crude aminoquinoline as an off-white iridescent solid (0.900 g, 100% with minor impurities); analytical data for this compound are as previously described.[29]

2-(Acetamido)-7-methylquinoline (25). Compound **24** (3.02 g, 19.1 mmol) was diluted with anhydrous THF (100 mL), N-acetylimidazole (2.52 g, 23.0 mmol) was added, and the mixture was heated at reflux for 17 h. The mixture was cooled, concentrated, and the residue was diluted with EtOAc (200 mL) and washed with H_2O (~500 mL) and sat. aq. NaCl (100 mL). The organic layer was dried over anhydrous sodium sulfate and concentrated. The residue was dissolved in a minimal amount of hot EtOAc and precipitated with hexanes (~200 mL) to yield **25** as a pale-tan iridescent solid (3.23 g, 85%) after washing with hexanes. Analytical data for this compound are consistent with those previously reported.[18,29]

General Procedure for the Synthesis and Deprotection of Phenyl Ether-Linked Aminoquinolines. Sodium hydride (60% suspension in mineral oil, 1 equiv) was diluted with anhydrous DMF (1–2 mL) and cooled to 0 °C under argon. A solution of the required phenol (1 equiv) in anhydrous DMF (1–2 mL) was added slowly to the suspension and stirred at 0 °C for 10–30 min (typically ~25 min), following which bromide **26** (1 equiv) was added as a solution in anhydrous DMF. The reaction mixture was stirred at 0 °C for 40 min–1 h (typically ~50 min) and quenched at 0 °C by addition of a 1:1 sat.

aq. NaCl/H_2O mixture (~15 mL) or a sat. aq. $NaHCO_3$ solution. The mixture was extracted with EtOAc (usually 3 × 20 mL was sufficient; for tertiary amines, more exhaustive extraction was required), and the organic phase was washed with 5% aq. NaCl ((3–4) × 30–80 mL) and sat aq. NaCl (30–50 mL). The organic layer was dried over anhydrous sodium sulfate, concentrated, and purified by flash column chromatography (12 g SiO_2 cartridge), using gradients as described for individual compounds below. The resulting intermediate acetamides were not characterized or purified further but were diluted with anhydrous MeOH (5–10 mL), and anhydrous K_2CO_3 (2–2.5 equiv) was added. The mixture was heated at reflux for 2–2.5, cooled, and concentrated. The resulting residue was partitioned between EtOAc and 1:1 H_2O/sat. aq. NaCl, and the aqueous layer was extracted with EtOAc ((2–3) × 5–20 mL). The organic layers were washed with sat. aq. NaCl and dried over anhydrous sodium sulfate. Purification is detailed under subheadings for individual compounds. The free aminoquinoline was diluted in dry ether (or 10:1 ether/MeOH) and filtered to remove any particulate matter. To the filtered solution, methanolic HCl (3 M, 1.5 mL) was added, and the mixture was stirred either 5 min (when a Boc group was not present) or overnight (when a Boc group was present). The hydrochloride salts were isolated by filtration, and the final purification was performed as described below for individual compounds.

7-[3-(2-(Dimethylamino)ethyl)phenoxy)methyl]quinolin-2-amine Dihydrochloride (6). This was prepared from **26** (0.150 g, 0.54 mmol) and phenol **29** (0.089 g, 0.54 mmol). Workup and purification by flash column chromatography, eluting with a gradient of 2% MeOH in EtOAc to 30% MeOH in EtOAc, afforded the intermediate acetamide **60** as a white semisolid (0.081 g, 41%) that was immediately deprotected using K_2CO_3 (0.062 g, 0.446 mmol). After workup, the resulting gum was dissolved in minimal EtOAc, and hexanes were added to precipitate a white solid. This procedure was repeated twice, and the solid was diluted with 10% MeOH in ether (10 mL), filtered, and concentrated. The resulting residue was diluted in ether (~10 mL) and treated with methanolic HCl for 5 min. Filtration afforded **6** (0.050 g, 57% from **64**) as a cream-colored powder after washing with ether (3 × 2 mL): mp 115–120 °C (softens), 240 °C (dec). ^{1}H NMR (500 MHz) DMSO-d_6: δ 14.37 (s, 1 H), 10.46 (s, 1 H), 9.21 (br s, 1 H), 8.38 (d, J = 9.3 Hz, 1 H), 8.22 (br s, 1 H), 7.95 (d, J = 8.2 Hz, 1 H), 7.78 (s, 1 H), 7.54 (dd, J = 8.2, 1.4 Hz, 1 H), 7.28 (t, J = 7.9 Hz, 1 H), 7.11 (d, J = 9.3 Hz, 1 H), 7.02 (d, J = 1.7 Hz, 1 H), 6.95 (dd, J = 8.0, 2.3 Hz, 1 H), 6.89 (d, J = 7.6 Hz, 1 H), 5.32 (s, 2 H), 3.29 (dt, J = 12.1, 4.6 Hz, 2 H), 3.01–2.98 (m, 2 H), 2.80 (s, 3 H), 2.79 (s, 3 H). ^{13}C- NMR (126 MHz; DMSO-d_6): δ 158.2, 154.4, 142.8, 142.3, 138.6, 135.8, 129.8, 129.0, 123.8, 121.5, 120.3, 115.5, 115.1, 113.7, 113.0, 68.4, 57.1, 42.1, 29.8; ESIMS m/z (rel. intensity) 322 (MH[+], 100). HRMS calcd for $C_{20}H_{24}N_3O$: 322.1919; found, 322.1912.

7-[3-(2-(Methylamino)ethyl)phenoxy)methyl]quinolin-2-amine Dihydrochloride (7). This was prepared from **26** (0.150 g, 0.54 mmol) and phenol **32** (0.138 g, 0.54 mmol). Workup and purification by flash column chromatography, eluting with a gradient of 5% EtOAc in CH_2Cl_2 to 40% EtOAc in CH_2Cl_2, afforded intermediate acetamide **61** as a white semisolid (0.181 g, 74%), which was immediately deprotected using K_2CO_3 (0.111g, 0.806 mmol). After workup, the resulting gum was triturated with hexanes and 1:1 ether/hexanes (5 mL each) and filtered to yield a white solid that was suspended in ether (8 mL) and treated with methanolic HCl (1.5 mL) for 20 h. Filtration afforded **7** (0.105 g, 69% from **61**) as a chalky white solid after trituration with 10% MeOH in ether (3 × 1 mL): mp 211.5–213 °C. ^{1}H NMR (500 MHz; DMSO-d_6): δ 14.48 (s, 1 H), 9.26 (br s, 1 H), 9.01 (s, 2 H), 8.37 (d, J = 9.3 Hz, 1 H), 8.27 (br s, 1 H), 7.95 (d, J = 8.2 Hz, 1 H), 7.78 (s, 1 H), 7.54 (dd, J = 8.2, 1.0 Hz, 1 H), 7.27 (t, J = 7.9 Hz, 1 H), 7.12 (d, J = 9.3 Hz, 1 H), 6.99 (s, 1 H), 6.94 (dd, J = 8.2, 2.4 Hz, 1 H), 6.87 (d, J = 7.6 Hz, 1 H), 5.32 (s, 2 H), 3.16–3.11 (m, 2 H), 2.93 (t, J = 8.0 Hz, 2 H), 2.55 (t, J = 5.4 Hz, 3 H). ^{13}C NMR (126 MHz; DMSO-d_6): δ 158.2, 154.4, 142.8, 142.3, 138.9, 135.8, 129.8, 129.0, 123.8, 121.4, 120.3, 115.4, 115.1, 113.7, 113.0, 68.4, 48.9, 32.3, 31.4; ESIMS m/z (rel. intensity) 308 (MH[+], 100). HRMS calcd for $C_{19}H_{22}N_3O$: 308.1763; found, 308.1760.

7-[3-(Dimethylamino)methyl)phenoxy)methyl]quinolin-2-amine Dihydrochloride (8). This was prepared from **26** (0.120 g, 0.42 mmol) and phenol **34** (0.065 g, 0.43 mmol). Workup and purification by flash column chromatography, eluting with a gradient of 2% MeOH in EtOAc to 30% MeOH in EtOAc, afforded intermediate acetamide **62** as a white gum (0.091 g, 61%), which was deprotected using K_2CO_3 (0.089g, 0.65 mmol). After workup, the resulting syrup was triturated with 5:1 DCM/hexanes (5 mL) to yield a white solid. This was diluted in EtOAc (3 mL), filtered to remove particulates, and concentrated. The residue was diluted in MeOH (1 mL) and treated with methanolic HCl (1.5 mL). Ether was added to precipitate a gum that was washed with 5% MeOH in ether and ether (1 mL each) to yield **8** (0.063 g, 64% from **62**) as a pale-yellow foam: mp 76 °C (softens), 91−94 °C (melts), 240 °C (dec). ^{1}H NMR (500 MHz; DMSO-d_6): δ 14.37 (s, 1 H), 10.77 (s, 1 H), 9.21 (br s, 1 H), 8.38 (d, J = 9.3 Hz, 1 H), 8.24 (s, 1 H), 7.95 (d, J = 8.2 Hz, 1 H), 7.78 (s, 1 H), 7.55 (dd, J = 8.2, 1.4 Hz, 1 H), 7.41−7.38 (m, 2 H), 7.15−7.10 (m, 3 H), 5.36 (s, 2 H), 4.24 (d, J = 5.3 Hz, 2 H), 2.68 (s, 3 H), 2.67 (s, 3 H). ^{13}C NMR (126 MHz; DMSO-d_6): δ 158.2, 154.4, 142.9, 142.1, 132.1, 130.1, 129.1, 124.0, 123.6, 120.4, 117.5, 115.9, 115.2, 113.9, 68.6, 59.4, 48.7, 41.6; ESIMS m/z (rel. intensity) 308 (MH$^+$, 100). HRMS calcd for $C_{19}H_{22}N_3O$: 308.1763; found, 308.1757.

7-[3-(Methylamino)methyl)phenoxy)methyl]quinolin-2-amine Dihydrochloride (9). This was prepared from **26** (0.150 g, 0.54 mmol) and phenol **35** (0.128 g, 0.54 mmol). Workup and purification by flash column chromatography, eluting with 5% EtOAc in CH_2Cl_2 to 33% EtOAc in CH_2Cl_2, afforded intermediate acetamide **63** as a colorless foam (0.184 g, 78%), which was deprotected using K_2CO_3 (0.117 g, 0.844 mmol). After workup, the resulting residue was diluted in ether (5 mL), filtered to remove particulates, and treated with methanolic HCl (1.5 mL) for 20 h. Ether (3 mL) was added, and the precipitate was filtered to yield **9** as a white amorphous solid (0.102 g, 66% from **63**) after trituration with 2:1 ether/MeOH (2 mL) and washing with ether (2 mL): mp 257−259 °C. ^{1}H NMR (500 MHz; DMSO-d_6): δ 14.41 (s, 1 H), 9.27 (s, 3 H), 8.37 (d, J = 9.3 Hz, 1 H), 8.30 (br s, 1 H), 7.95 (d, J = 8.2 Hz, 1 H), 7.78 (s, 1 H), 7.55−7.53 (m, 1 H), 7.37 (t, J = 7.9 Hz, 1 H), 7.33 (s, 1 H), 7.12−7.08 (m, 3 H), 5.35 (s, 2 H), 4.08 (t, J = 5.5 Hz, 2 H), 2.52 (d, J = 5.2 Hz, 3 H, partially obscured by solvent signal). ^{13}C NMR (126 MHz; DMSO-d_6): δ 158.1, 154.4, 142.8, 142.1, 135.8, 133.6, 129.9, 129.0, 123.8, 122.5, 120.3, 116.6, 115.14, 115.10, 113.8, 68.5, 51.0, 31.9; ESIMS m/z (rel. intensity) 294 (MH$^+$, 100). HRMS calcd for $C_{18}H_{20}N_3O$: 294.1606; found, 294.1603.

7-[3-Aminomethyl)phenoxy)methyl]quinolin-2-amine Dihydrochloride (10). This was prepared from **26** (0.100 g, 0.358 mmol) and phenol **37** (0.080 g, 0.358 mmol). Workup and purification by flash column chromatography, eluting with 5% EtOAc in CH_2Cl_2 to 50% EtOAc in CH_2Cl_2, afforded intermediate acetamide **64** as a colorless foam (0.121 g, 80%), which was deprotected using K_2CO_3 (0.079 g, 0.569 mmol). After workup, the resulting gum was triturated with 5:1 ether/hexanes and 2:1 hexanes/EtOAc (5 mL each) to yield the product as a white solid, which was diluted in MeOH, filtered to remove particulates, and concentrated. The residue was diluted in ether (8 mL) and treated with methanolic HCl (1.5 mL) for 20 h. The precipitate was filtered to yield **10** as a white powder (0.050 g, 50% from **64**) after trituration with 15% MeOH in ether (2 × 2 mL) and 2:1 ether/MeOH (2 mL) and washing with ether (2 mL): mp 254−255 °C. ^{1}H NMR (500 MHz; DMSO-d_6): δ 14.49 (s, 1 H), 9.24 (br s, 1 H), 8.45 (s, 3 H), 8.37 (d, J = 9.3 Hz, 1 H), 8.28 (br s, 1 H), 7.95 (d, J = 8.2 Hz, 1 H), 7.78 (s, 1 H), 7.54 (dd, J = 8.2, 1.4 Hz, 1 H), 7.35 (t, J = 7.9 Hz, 1 H), 7.28 (d, J = 1.8 Hz, 1 H), 7.13−7.05 (m, 3 H), 5.34 (s, 2 H), 3.99 (q, J = 5.7 Hz, 2 H). ^{13}C NMR (126 MHz; DMSO-d_6): δ 158.1, 154.4, 142.8, 142.1, 135.82, 135.69, 129.8, 129.0, 123.8, 121.5, 120.3, 115.7, 115.1, 114.6, 113.8, 68.5, 42.1; ESIMS m/z (rel. intensity) 280 (MH$^+$, 100). HRMS calcd for $C_{17}H_{18}N_3O$: 280.1450; found, 280.1442.

7-[(Pyridin-3-yloxy)methyl]quinolin-2-amine Dihydrochloride (11). This was prepared from **26** (0.120 g, 0.43 mmol) and 3-hydroxypyridine (0.041 g, 0.43 mmol). Workup and purification by trituration with 50% CH_2Cl_2 in hexanes (4 mL) afforded intermediate acetamide **74** as a flocculent, peach-colored solid (0.068 g, 54%),

which was deprotected using K_2CO_3 (0.064 g, 0.466 mmol). After workup, the resulting residue was triturated with DCM/hexanes (~4 mL), and the pale-yellow iridescent solid was collected, dissolved in MeOH, filtered to remove particulates, and concentrated. The residue was resuspended in MeOH (1 mL), and methanolic HCl (1.5 mL) was added. After 5 min, the addition of ether (5 mL) precipitated **11** as an off-white solid (0.067 g, 88% from **74**) after washing with ether (2 mL): mp 188 °C (softens), 211−214 °C (melts). ^{1}H NMR (500 MHz; DMSO-d_6): δ 14.35 (s, 1 H), 9.23 (br s, 1 H), 8.65 (s, 1 H), 8.43 (s, 1 H), 8.38 (d, J = 9.3 Hz, 1 H), 8.27 (br s, 1 H), 7.98−7.97 (m, 2 H), 7.79 (s, 1 H), 7.76−7.74 (m, 1 H), 7.57 (d, J = 8.1 Hz, 1 H), 7.13−7.11 (m, 1 H), 5.51 (s, 2 H); the pyridinium N−H proton is broadened into the baseline and is not visible; ^{13}C NMR (126 MHz; DMSO-d_6): δ 155.7, 154.6, 143.0, 140.9, 138.2, 135.9, 133.6, 129.3, 127.7, 126.5, 124.2, 120.7, 115.7, 114.2, 69.7; ESIMS m/z (rel. intensity) 252 (MH$^+$, 100). HRMS calcd for $C_{15}H_{14}N_3O$: 252.1137; found, 252.1130.

7-((3-(Dimethylamino)phenoxy)methyl)quinolin-2-amine Dihydrochloride (12). This was prepared from **26** (0.120 g, 0.43 mmol) and 3-(dimethylamino)phenol (0.041 g, 0.43 mmol). After workup, the resulting residue was purified by flash column chromatography, eluting with a gradient of 5% EtOAc in CH_2Cl_2 to 25% EtOAc in CH_2Cl_2, to yield intermediate acetamide **65** (0.070 g, 49%) as a clear syrup, which was immediately deprotected using K_2CO_3 (0.058 g, 0.42 mmol). After workup, the resulting oil was treated with methanolic HCl (4 mL), and ether (12 mL) was added to afford an off-white solid; an analytically pure sample for assay was prepared by preparative LC-MS, using the instrument described in the General Procedures section and a Phenomenex Luna 5 μm C8(2) 100 Å, 150 × 21.2 mm preparative HPLC column, eluting with a gradient of 95% H_2O + 0.1% formic acid/5% MeCN + 0.1% formic acid to 81% H_2O + 0.1% formic acid/19% MeCN + 0.1% formic acid over 20 min. Evaporation of the desired mass fraction and retreatment with methanolic HCl (1 mL) and ether (1 mL) afforded **12** as a white solid (0.023 g, 30% from **65**): mp 195−197 °C. ^{1}H NMR (500 MHz; DMSO-d_6): δ 14.30 (s, 1 H), 9.22 (br s, 1 H), 8.38 (d, J = 9.5 Hz, 1 H), 8.22 (br s, 1 H), 7.95 (d, J = 9.0 Hz, 1 H), 7.77 (s, 1 H), 7.55 (d, J = 9.0 Hz, 1 H), 7.27 (s, 1 H), 7.11 (d, J = 9.0 Hz, 1 H), 6.68 (br s, 3 H), 5.32 (s, 2 H), 2.99 (s, 6 H); one proton is not visible due to baseline broadening; ^{13}C NMR (126 MHz; DMSO-d_6): δ 159.4, 154.8, 143.4, 142.9, 136.3, 130.6, 129.4, 124.4, 120.8, 115.6, 114.2, 66.9; four of the aryl carbons are not visible due to baseline broadening, and the methyl carbon signals are obscured by the solvent peak; ESIMS m/z (rel. intensity) 294 (MH$^+$, 100). HRMS calcd for $C_{18}H_{20}N_3O$, 294.1606; found, 294.1599.

7-[3-(3-(Dimethylamino)propyl)phenoxy)methyl]quinolin-2-amine Dihydrochloride (13). This was prepared from **26** (0.150 g, 0.54 mmol) and phenol **49** (0.097 g, 0.54 mmol). Workup and purification by flash column chromatography, eluting with a gradient of 2% MeOH in EtOAc to 40% MeOH in EtOAc, afforded intermediate acetamide **66** as a pale yellow gum (0.105 g, 51%) after filtering an EtOAc solution to remove particulates and reconcentrating. The intermediate acetamide was deprotected using K_2CO_3 (0.077 g, 0.556 mmol). After workup, the resulting residue was diluted in CH_2Cl_2 (1 mL) and precipitated with hexanes (5 mL) to yield the free aminoquinoline as a white solid, which was diluted with CH_2Cl_2, filtered again, and concentrated. The residue was diluted in ether (5 mL) and treated with methanolic HCl (1 mL) for 5 min. The mixture was then concentrated, and the residue was triturated with ether (2 × 5 mL), 10% MeOH in ether (4 × 5 mL), and EtOAc (5 mL), to yield **13** as an off-white foam (0.045 g, 40% from **66**): mp 72−75 °C (softens), 260 °C (dec). ^{1}H NMR (500 MHz; DMSO-d_6): δ 14.34 (s, 1 H), 10.41 (s, 1 H), 9.17 (br s, 1 H), 8.37 (d, J = 9.3 Hz, 1 H), 8.21 (br s, 1 H), 7.95 (d, J = 8.2 Hz, 1 H), 7.77 (s, 1 H), 7.54 (dd, J = 8.2, 1.3 Hz, 1 H), 7.24 (t, J = 7.9 Hz, 1 H), 7.10 (d, J = 9.3 Hz, 1H), 6.96 (t, J = 1.8 Hz, 1 H), 6.90−6.88 (m, 1 H), 6.85 (d, J = 7.7 Hz, 1 H), 5.31 (s, 2 H), 3.02−2.99 (m, 2 H), 2.72 (s, 3 H), 2.72 (s, 3 H), 2.61 (t, J = 7.7 Hz, 2 H), 2.00−1.94 (m, 2 H). ^{13}C NMR (126 MHz; DMSO-d_6): δ 158.1, 154.4, 142.8, 142.36, 142.27, 135.9, 129.6, 129.0, 123.8, 121.1, 120.3, 115.12, 115.01, 113.7, 112.3, 68.3, 56.1, 42.0, 31.9,

25.1; ESIMS *m/z* (rel. intensity) 336 (MH⁺, 100). HRMS calcd for C₂₁H₂₆N₃O, 336.2076; found, 336.2073.

7-((3-(2-(Dimethylamino)ethoxy)phenoxy)methyl)quinolin-2-amine Dihydrochloride (14). This was prepared from **26** (0.100 g, 0.36 mmol) and phenol **42** (0.065 g, 0.36 mmol). After workup, the resulting residue was purified by flash column chromatography, eluting with 50% EtOAc in hexanes + 5% Et₃N, to yield intermediate acetamide **67** (0.050 g, 37%) as an opaque syrup, which was immediately deprotected using K₂CO₃ (0.036 g, 0.26 mmol). After workup, the resulting oil was treated with methanolic HCl (3 M, 3 mL), and ether (9 mL) was added, affording an off-white solid; an analytically pure sample for assay was prepared by preparative LC-MS, using the instrument described in the General Procedures section and a Phenomenex Luna 5 *μ*m C8(2) 100 Å, 150 × 21.2 mm preparative HPLC column, eluting with a gradient of 99% H₂O + 0.1% formic acid/1% MeCN + 0.1% formic acid to 98% H₂O + 0.1% formic acid 2% MeCN + 0.1% formic acid over 20 min. Evaporation of the desired mass fraction and retreatment with methanolic HCl (1 mL) and ether (1 mL) afforded **14** as a white solid (0.0065 g, 12%, from **67**): mp 181−183 °C. ¹H NMR (500 MHz; DMSO-*d₆*): δ 14.43 (s, 1 H), 10.57 (s, 1 H), 9.24 (br s, 1 H), 8.37 (d, *J* = 9.0 Hz, 1 H), 8.23 (br s, 1 H), 7.95 (d, *J* = 8.0 Hz, 1 H), 7.77 (s, 1 H), 7.53 (d, *J* = 8.0 Hz, 1 H), 7.24 (dd, *J* = 8.0, 8.0 Hz, 1 H), 7.11 (d, *J* = 9.0 Hz, 1 H), 6.72−6.67 (m, 2 H), 6.62 (dd, *J* = 8.0, 2.5 Hz, 1 H), 5.32 (s, 2 H), 4.36 (t, *J* = 5.0 Hz, 2 H), 3.48 (dt, *J* = 5.0, 5.0 Hz, 2 H), 2.83 (s, 6 H). ¹³C NMR (126 MHz; DMSO-*d₆*): δ 159.7, 159.2, 154.9. 143.2, 142.6, 136.3, 130.7, 129.5, 124.2, 120.8, 115.8, 114.2, 108.2, 108.0, 102.5, 69.0, 62.8, 55.7, 48.2. ESIMS *m/z* (rel. intensity) 338 (MH⁺, 100). HRMS calcd for C₂₀H₂₄N₃O₂, 338.1868; found, 338.1864.

7-[[4-(Dimethylamino)methyl]phenoxy]methyl]quinolin-2-amine Dihydrochloride (15). This was prepared from **26** (0.120 g, 0.43 mmol) and phenol **44** (0.065 g, 0.43 mmol). Workup and purification by flash column chromatography, eluting with a gradient of 3% MeOH in EtOAc to 20% MeOH in EtOAc, afforded crude acetamide **68** as a foamy pale-yellow semisolid (0.099 g, 66%), which was deprotected using K₂CO₃ (0.078 g, 0.57 mmol). After workup, the resulting yellowish gum was triturated with 10% EtOAc in hexanes (10 mL), diluted with MeOH, filtered, and reconcentrated. The resulting residue was diluted with ether (5 mL) and treated with methanolic HCl (1 mL) for 5 min. Concentration afforded an off-white foamy solid; an analytically pure sample for assay was prepared by preparative LC-MS, using the instrument described in the General Procedures section and a Phenomenex Luna 5 *μ*m C8(2) 100 Å, 150 × 21.2 mm preparative HPLC column, eluting with a gradient of 95% H₂O + 0.1% formic acid/5% MeCN + 0.1% formic acid to 80% H₂O + 0.1% formic acid 20% MeCN + 0.1% formic acid over 20 min. Evaporation of the desired mass fraction yielded a syrup that was suspended in MeOH (2 mL), filtered, concentrated, and treated with methanolic HCl (0.7 mL). Ether (5 mL) was added to precipitate **15**, which was obtained as a white hygroscopic solid (0.022 g, 21% from **68**) after washing with ether and drying: mp 251−253.5 °C. ¹H NMR (500 MHz; DMSO-*d₆*): δ 14.27 (s, 1 H), 10.50 (s, 1 H), 9.15 (br s, 1 H), 8.37 (d, *J* = 9.3 Hz, 1 H), 8.21 (br s, 1 H), 7.95 (d, *J* = 8.2 Hz, 1 H), 7.76 (s, 1 H), 7.55−7.54 (m, 1 H), 7.50 (d, *J* = 8.7 Hz, 2 H), 7.12 (d, *J* = 8.7 Hz, 2 H), 7.10 (d, *J* = 9.4 Hz, 1 H), 5.35 (s, 2 H), 4.19 (d, *J* = 4.7 Hz, 2 H), 2.66 (s, 3 H), 2.65 (s, 3 H). ¹³C NMR (126 MHz; DMSO-*d₆*): δ 158.8, 154.4, 142.8, 142.0, 135.9, 132.7, 129.0, 123.8, 122.8, 120.4, 115.22, 115.02, 113.8, 68.5, 58.9, 41.3; ESIMS *m/z* (rel. intensity) 308 (MH⁺, 100). HRMS calcd for C₁₉H₂₂N₃O, 308.1763; found, 308.1756.

7-[[4-(Methylamino)methyl]phenoxy]methyl]quinolin-2-amine Dihydrochloride (16). This was prepared from **26** (0.150 g, 0.54 mmol) and phenol **45** (0.128 g, 0.54 mmol). Workup and purification by flash column chromatography, eluting with a gradient of 5% EtOAc in CH₂Cl₂ to 33% EtOAc in CH₂Cl₂, afforded intermediate acetamide **69** as a pale yellow foam (0.184 g, 78%), which was deprotected using K₂CO₃ (0.117 g, 0.844 mmol). After workup, the resulting residue was purified by flash column chromatography, eluting with a gradient of EtOAc to 2% MeOH in EtOAc, to yield a colorless foam. The free aminoquinoline was diluted with ether (7 mL) and treated with methanolic HCl (1.5 mL) for 18 h. The precipitate was filtered to yield

16 as a white chalky solid (0.131 g, 85% from **69**) after washing with 20% MeOH in ether (5 mL) and drying: mp 283−285 °C. ¹H NMR (500 MHz; DMSO-*d₆*): δ 14.31 (s, 1 H), 9.07 (br s, 3 H), 8.36 (d, *J* = 9.3 Hz, 1 H), 8.29 (br s, 1 H), 7.94 (d, *J* = 8.2 Hz, 1 H), 7.75 (s, 1 H), 7.53 (dd, *J* = 8.2, 1.3 Hz, 1 H), 7.47−7.45 (m, 2 H), 7.10−7.09 (m, 3 H), 5.35 (s, 2 H), 4.03 (t, *J* = 5.6 Hz, 2 H), 2.48 (m, 3 H, partially obscured by solvent peak). ¹³C NMR (126 MHz; DMSO-*d₆*): δ 158.4, 154.4, 142.7, 142.0, 136.0, 131.6, 129.0, 124.5, 123.7, 120.4, 115.2, 114.9, 113.7, 68.5, 50.6, 31.7; ESIMS *m/z* (rel. intensity) 294 (MH⁺, 100). HRMS calcd for C₁₈H₂₀N₃O, 294.1606; found, 294.1597.

7-[[(3-((Dimethylamino)methyl)phenyl)amino]methyl]quinolin-2-amine Trihydrochloride (17). Aldehyde **81** (0.080 g, 0.374 mmol) and aniline **48** (0.067 g, 0.449 mmol) were diluted in abs. EtOH (12 mL), and anhydrous Na₂SO₄ (~0.5 g) was added. The mixture was heated to 60 °C for 1 h, glacial AcOH (8 *μ*L) was added, and heating was continued for 22 h. The mixture was cooled to room temperature, and NaBH₄ (0.018 g, 0.486 mmol) was added, and after 20 min, the mixture was filtered. The filtrate was evaporated and partitioned between EtOAc and sat. aq. NaHCO₃ (20 mL each). The aqueous layer was extracted with EtOAc (2 × 30 mL), and the organic layer was washed with H₂O and sat. aq. NaCl (20 mL each), dried over anhydrous sodium sulfate, and concentrated. The resulting residue was purified by flash column chromatography, eluting with a gradient of CH₂Cl₂ to 25% MeOH in CH₂Cl₂, to yield the crude acetamide as a white solid (0.032 g, 25%) after trituration with 10% CH₂Cl₂ in hexanes. The intermediate acetamide was deprotected using K₂CO₃ (0.026 g, 0.188 mmol) and worked up using the general procedure; the obtained yellow gum was triturated with 10% EtOAc in hexanes and hexanes (3 mL each), diluted with 20% MeOH in ether (~5 mL), and treated with methanolic HCl (0.5 mL) for 5 min. The precipitate was collected, diluted in MeOH (0.5 mL), and precipitated with ether (3 mL) to afford **17** (0.019 g, 12% from the acetamide) as a pale-yellow powder: mp 219−221 °C. ¹H NMR (500 MHz; DMSO-*d₆*): δ 14.18 (s, 1 H), 10.35 (s, 1 H), 9.11 (br s, 1 H), 8.33 (d, *J* = 9.3 Hz, 1 H), 8.12 (br s, 1 H), 7.87 (d, *J* = 8.2 Hz, 1 H), 7.64 (s, 1 H), 7.48 (dd, *J* = 8.2, 1.3 Hz, 1 H), 7.11 (t, *J* = 7.8 Hz, 1 H), 7.04 (d, *J* = 9.3 Hz, 1 H), 6.75 (s, 1 H), 6.68 (d, *J* = 7.5 Hz, 1 H), 6.63 (dd, *J* = 8.2, 1.6 Hz, 1 H), 4.49 (s, 2 H), 4.07 (d, *J* = 5.5 Hz, 2 H), 2.63 (s, 3 H), 2.62 (s, 3 H); the anilinium N−H protons appear as a broad singlet, exchanging with residual water at 4.2 ppm. ¹³C NMR (126 MHz; DMSO-*d₆*): δ 154.3, 148.5, 145.9, 142.9, 135.8, 131.1, 129.4, 128.8, 124.3, 119.8, 118.3, 114.7, 114.1, 113.5, 113.1, 60.0, 46.1, 41.5; ESIMS *m/z* (rel. intensity) 307 (MH⁺, 100). HRMS calcd for C₁₉H₂₃N₄, 307.1923; found, 307.1916.

7-[[(3-((Methylamino)methyl)phenyl)amino]methyl]quinolin-2-amine Trihydrochloride (18). Bromide **26** (0.092 g, 0.330 mmol), aniline **50** (0.195 g, 0.826 mmol), and KI (0.006 g, 15 mol %) were combined in anhydrous MeCN (2.5 mL), sealed, and heated under microwave irradiation at 110 °C for 20 min. The mixture was diluted with CH₂Cl₂ (30 mL) and washed with sat. aq. NaHCO₃ (20 mL). The aqueous layer was extracted with CH₂Cl₂ (20 mL), and the organic layers were washed with H₂O and sat. aq. NaCl (30 mL), dried over anhydrous sodium sulfate, and concentrated. The residue was purified by flash column chromatography, eluting with a gradient of 5% EtOAc in CH₂Cl₂ to 40% EtOAc in CH₂Cl₂, to yield intermediate acetamide **75** as a yellow foam (0.103 g, 72%), which was deprotected using K₂CO₃ (0.065 g, 0.474 mmol) and worked up according to the general procedure. The resulting residue was purified by flash column chromatography, eluting with a gradient of EtOAc to 2% MeOH in EtOAc, to yield a pale-yellow foam. The free aminoquinoline was diluted with 30% MeOH in ether (11 mL) and was treated with methanolic HCl (1.5 mL) for 20 h. The precipitate was collected and precipitated from hot MeOH (0.5 mL) with ether (5 mL) to yield **18** as a cream-colored solid (0.050 g, 53% from **75**): mp 230−232 °C. ¹H NMR (500 MHz; DMSO-*d₆*): δ14.30 (s, 1 H), 9.10 (br s, 3 H), 8.34 (d, *J* = 9.3 Hz, 1 H), 8.16 (br s, 1 H), 7.88 (d, *J* = 8.2 Hz, 1 H), 7.65 (s, 1 H), 7.49 (dd, *J* = 8.2, 1.3 Hz, 1 H), 7.09 (t, *J* = 7.8 Hz, 1 H), 7.06 (d, *J* = 9.3 Hz, 1 H), 6.76 (s, 1 H), 6.68 (d, *J* = 7.5 Hz, 1 H), 6.60 (dd, *J* = 8.1, 1.7 Hz, 1 H), 4.49 (s, 2 H), 3.92 (t, *J* = 5.9 Hz, 2 H), 2.47 (t, *J* = 5.4 Hz, 3 H, partially obscured by solvent peak); the anilinium N−H

protons appear as a broad singlet, exchanging with residual water at 4.4 ppm. ^{13}C NMR (126 MHz; DMSO-d_6): δ 154.5, 148.5, 146.1, 143.0, 136.0, 132.9, 129.5, 129.0, 124.4, 120.0, 117.6, 114.9, 113.6, 113.24, 113.19, 51.7, 46.4, 32.1; ESIMS m/z (rel. intensity) 293 (MH$^+$, 100). HRMS calcd for $C_{18}H_{21}N_4$, 293.1766; found, 293.1760.

7-[(4-Fluoro-3-((methylamino)methyl)phenoxy)methyl]quinolin-2-amine Dihydrochloride (19). This was prepared from **26** (0.100 g, 0.358 mmol) and phenol **54** (0.091 g, 0.358 mmol). Workup and purification by flash column chromatography, eluting with 2% EtOAc in CH$_2$Cl$_2$ to 30% EtOAc in CH$_2$Cl$_2$ afforded intermediate acetamide **70** as a colorless foam (0.128 g, 79%), which was immediately deprotected using K$_2$CO$_3$ (0.078 g, 0.564 mmol). After workup, the resulting gum was triturated with hexanes (2 × 5 mL), diluted in 10% MeOH in ether (9 mL), and treated with methanolic HCl (1.5 mL) for 20 h. The precipitate was collected and precipitated 3 times from hot MeOH (0.5 mL) with ether (2.5 mL) to yield **19** as a white amorphous solid (0.053 g, 49% from **70**): mp 293−294 °C. ^{1}H NMR (500 MHz; DMSO-d_6): δ 14.35 (s, 1 H), 9.29 (br s, 3 H), 8.37 (d, J = 9.3 Hz, 1 H), 8.29 (br s, 1 H), 7.95 (d, J = 8.2 Hz, 1 H), 7.78 (s, 1 H), 7.54 (dd, J = 8.2, 1.3 Hz, 1 H), 7.44 (dd, J = 6.0, 3.1 Hz, 1 H), 7.27 (t, J = 9.2 Hz, 1 H), 7.14 (dt, J = 8.9, 3.6 Hz, 1 H), 7.10 (d, J = 9.3 Hz, 1 H), 5.33 (s, 2 H), 4.14 (s, 2 H), 2.57 (s, 3 H). ^{13}C NMR (126 MHz; DMSO-d_6): δ (156.0 + 154.04, 1 C), 154.4, (154.11 + 154.10, 1 C), 142.8, 141.8, 136.0, 129.0, 123.8, 120.4, (119.89 + 119.76, 1 C), (118.18 + 118.15, 1 C), (117.10 + 117.03, 1C), (116.53 + 116.35, 1 C), 115.3, 113.8, 69.2, (44.44 + 44.41, 1 C), 32.2; ESIMS m/z (rel. intensity) 312 (MH$^+$, 100). HRMS calcd for $C_{18}H_{19}FN_3O$, 312.1512; found, 312.1502.

7-[(4-Chloro-3-((methylamino)methyl)phenoxy)methyl]quinolin-2-amine Dihydrochloride (20). This was prepared from **26** (0.100 g, 0.358 mmol) and phenol **55** (0.097 g, 0.358 mmol). Workup and purification by flash column chromatography, eluting with 2% EtOAc in CH$_2$Cl$_2$ to 30% EtOAc in CH$_2$Cl$_2$ afforded intermediate acetamide **71** as a colorless foam (0.136 g, 81%), which was deprotected using K$_2$CO$_3$ (0.080 g, 0.578 mmol). After workup, the resulting gum was triturated with hexanes (2 × 5 mL), diluted in 10% MeOH in ether (9 mL), and treated with methanolic HCl (1.5 mL) for 20 h. The precipitate was collected and precipitated 4 times from hot MeOH (1 mL) with ether (3 mL) to yield **20** as a white amorphous solid (0.059 g, 51% from **71**): mp 290−291.5 °C (dec). ^{1}H NMR (500 MHz; DMSO-d_6): δ 14.36 (s, 1 H), 9.21 (br s, 3 H), 8.37 (d, J = 9.3 Hz, 1 H), 8.27 (br s, 1 H), 7.95 (d, J = 8.2 Hz, 1 H), 7.77 (s, 1 H), 7.54 (dd, J = 5.2, 2.2 Hz, 2 H), 7.49 (d, J = 8.9 Hz, 1 H), 7.14 (dd, J = 8.9, 3.0 Hz, 1 H), 7.10 (d, J = 9.3 Hz, 1 H), 5.37 (s, 2 H), 4.21 (s, 2 H), 2.60 (s, 3 H). ^{13}C NMR (126 MHz; DMSO-d_6): δ 156.9, 154.4, 142.7, 141.5, 135.9, 130.9, 130.5, 129.1, 124.9, 123.8, 120.4, 118.3, 117.0, 115.4, 113.8, 69.0, 48.3, 32.4; ESIMS m/z (rel. intensity) 328 (MH$^+$, 100). HRMS calcd for $C_{18}H_{19}ClN_3O$, 328.1217; found, 328.1212.

7-[((5-((Methylamino)methyl)pyridin-3-yl)oxy)methyl]quinolin-2-amine Trihydrochloride (21). This was prepared from **26** (0.100 g, 0.358 mmol) and phenol **59** (0.085 g, 0.358 mmol). Workup and purification by flash column chromatography, eluting with 15% EtOAc in CH$_2$Cl$_2$ to 90% EtOAc in CH$_2$Cl$_2$ afforded intermediate acetamide **73** as a white amorphous solid (0.098 g, 63%), which was deprotected using K$_2$CO$_3$ (0.062 g, 0.449 mmol). After workup, the resulting gum was triturated with hexanes (2 × 5 mL), diluted in 10% MeOH in ether (9 mL), and treated with methanolic HCl (1.5 mL) for 20 h. The precipitate was collected and precipitated from hot MeOH (0.5 mL) with ether (2.5 mL) to yield **21** as a flocculent, cream-colored solid (0.056 g, 62% from **73**): mp 224−226 °C. ^{1}H NMR (500 MHz; DMSO-d_6): δ 14.36 (s, 1 H), 9.47 (s, 2 H), 9.23 (br s, 1 H), 8.51 (d, J = 2.7 Hz, 1 H), 8.38 (d, J = 9.4 Hz, 2 H), 8.26 (br s, 1 H), 7.97 (d, J = 8.2 Hz, 2 H), 7.80 (s, 1 H), 7.56 (dd, J = 8.2, 1.4 Hz, 1 H), 7.11 (d, J = 9.3 Hz, 1 H), 5.46 (s, 2 H), 4.18 (t, J = 5.8 Hz, 2 H), 2.54 (t, J = 5.4 Hz, 3 H). ^{13}C NMR (126 MHz; DMSO-d_6): δ 154.54, 154.42, 143.0, 142.3, 141.2, 137.1, 136.0, 129.51, 129.32, 125.2, 124.2, 120.7, 115.6, 114.1, 69.4, 48.3, 32.1; ESIMS m/z (rel. intensity) 295 (MH$^+$, 100). HRMS calcd for $C_{17}H_{19}N_4O$, 295.1559; found, 295.1553.

(RS)-7-[(3-(1-(Methylamino)ethyl)phenoxy)methyl]quinolin-2-amine Ditrifluoroacetate (22). This was prepared from **26** (0.100 g,

0.36 mmol) and phenol **56** (0.090 g, 0.36 mmol). After workup, the resulting residue was purified by flash column chromatography, eluting with a gradient of 7% EtOAc in CH$_2$Cl$_2$, to 30% EtOAc in CH$_2$Cl$_2$ to yield intermediate acetamide **72** as a white solid (0.119 g, 74%), which was immediately deprotected using K$_2$CO$_3$ (0.073 g, 0.53 mmol). After workup, the resulting oil was treated with trifluoroacetic acid (∼0.3 mL) in ether (5 mL) and stirred at room temperature 18 h to afford **22** as a white solid (0.077 g, 50% from **72**): mp 120−123 °C. ^{1}H NMR (500 MHz; DMSO-d_6): δ 14.37 (s, 1 H), 9.15 (s, 1 H), 8.92 (br s, 2 H), 8.39 (d, J = 9.5 Hz, 1 H), 7.97 (d, J = 8.5 Hz, 1 H), 7.72 (s, 1 H), 7.56 (d, J = 9.5 Hz, 1 H), 7.42 (dd, J = 8.0, 8.0 Hz, 1 H), 7.23 (dd, J = 2.0, 1.5 Hz, 1 H), 7.14−7.05 (m, 3 H), 5.34 (s, 2 H), 4.30 (q, J = 6.0 Hz, 1 H), 2.44 (t, J = 5.0 Hz, 3 H), 1.54 (d, J = 6.0 Hz, 3 H); ^{13}C NMR (126 MHz, DMSO-d_6) δ (159.5 + 159.2 + 159.0 + 158.7, 1 C), 158.8, 155.1, 143.3, 142.4, 139.1, 136.7, 130.8, 129.5, 124.3, 120.9, 120.7, 115.7, 115.6, 114.8, 114.4, 103.5, 69.1, 58.3, 30.9, 19.3; ESIMS m/z (rel. intensity) 308 (MH$^+$, 100). HRMS calcd for $C_{19}H_{22}N_3O$, 308.1763; found, 308.1755.

(E)-Methyl 4-(2-Cyanovinyl)-3-nitrobenzoate (77).[23] Compound **76** (2.00 g, 9.56 mmol) was diluted in anhydrous CH$_2$Cl$_2$ (24 mL) and cooled to −15 °C. (Triphenylphosphoranylidene)acetonitrile (3.08 g, 10.2 mmol) was diluted in anhydrous CH$_2$Cl$_2$ (30 mL) and added to the reaction mixture dropwise over 50 min. The mixture was stirred a total of 90 min, warmed to room temperature, and concentrated. The residue was purified by flash column chromatography, eluting with a gradient of 10% EtOAc in hexanes to 35% EtOAc in hexanes. Fractions containing pure **77** were saved, and the remaining eluate was concentrated and repurified using the same column gradient to yield **77** as a white flocculent solid (1.76 g, 79%); ^{1}H NMR (500 MHz, CDCl$_3$) δ 8.72 (d, J = 1.7 Hz, 1 H), 8.32 (dd, J = 8.1, 1.7 Hz, 1 H), 7.87 (d, J = 8.1 Hz, 1 H), 7.69 (d, J = 11.8 Hz, 1 H), 5.77 (d, J = 11.8 Hz, 1 H), 3.94 (s, 3 H); ^{13}C NMR (126 MHz, CDCl$_3$) δ 164.2, 147.1, 145.7, 134.7, 133.3, 132.8, 131.1, 126.2, 115.6, 101.5, 53.0; ESIMS m/z (rel. intensity) 233 (MH$^+$, 100).

Methyl 2-Aminoquinoline-7-carboxylate (78).[23] Compound **77** (2.2 g, 9.47 mmol) was diluted in DMF/glacial AcOH (1:1, 20 mL), and one portion of iron powder (1.85 g, 33.2 mmol, divided into two roughly equal amounts) was added in smaller portions. The mixture was heated to 100 °C for 90 min, after which the second portion of iron was added in smaller portions. After a total of 2 h 50 min of heating, the mixture was cooled, concentrated to dryness, and the mixture was treated with sat. aq. NaHCO$_3$ (100 mL). This mixture was exhaustively extracted with EtOAc (total, 700 mL), and the organic phase was washed with sat. aq. NaCl (200 mL), dried over anhydrous sodium sulfate, and concentrated. The resulting yellow residue was diluted with EtOAc (10 mL) and heated until dissolution occurred. Hexanes (100 mL) were then added, and the mixture was sonicated vigorously until a precipitate formed. The precipitate was collected and washed with hexanes to yield **78** as a pale-yellow crystalline solid (1.59 g, 83%). ^{1}H NMR (500 MHz, CDCl$_3$) δ 8.40 (s, 1 H), 7.96 (d, J = 8.8 Hz, 1 H), 7.91 (dd, J = 8.3, 1.6 Hz, 1 H), 7.70 (d, J = 8.3 Hz, 1 H), 6.87 (d, J = 8.8 Hz, 1 H), 5.19 (s, 2 H), 3.99 (s, 3 H); ^{13}C NMR (126 MHz, CDCl$_3$) δ 167.0, 157.1, 146.0, 138.2, 131.4, 127.8, 127.6, 126.1, 122.8, 113.8, 52.4; ESIMS m/z (rel. intensity) 203 (MH$^+$, 100).

Methyl 2-Acetamidoquinoline-7-carboxylate (79). Compound **78** (1.89 g, 9.37 mmol) was diluted with anhydrous dioxane (60 mL), and *N*-acetylimidazole (1.24 g, 11.2 mmol) and a catalytic amount (∼0.050 g) of DMAP were added. The mixture was heated at 100 °C for 19 h, cooled, and concentrated, and the resulting residue was suspended in CH$_2$Cl$_2$ (300 mL). The organic layer was washed with H$_2$O (200 mL), and the aqueous layer was extracted with CH$_2$Cl$_2$ (2 × 200 mL). The organic layers were washed with H$_2$O (400 mL) and sat. aq. NaCl (300 mL), dried over anhydrous sodium sulfate, and concentrated. The residue was diluted in CH$_2$Cl$_2$ (10 mL), and hexanes (150 mL) were added until a precipitate formed. This was collected and dried to yield **79** as a tan iridescent solid (2.08 g, 91%): mp 218−219.5 °C. ^{1}H NMR (500 MHz, CDCl$_3$) δ 8.68 (br s, 1 H), 8.56−8.49 (m, 2 H), 8.22 (d, J = 9.0 Hz, 1 H), 8.06 (dd, J = 8.4, 1.7 Hz, 1 H), 7.85 (d, J = 8.4 Hz, 1 H), 4.00 (s, 3 H), 2.28 (s, 3 H); ^{13}C NMR (126 MHz, CDCl$_3$) δ

O

169.3, 166.8, 151.8, 145.8, 138.4, 131.4, 129.8, 128.7, 127.9, 124.7, 116.2, 52.5, 24.9; ESIMS m/z (rel. intensity) 245 (MH$^+$, 100).

N-(7-(Hydroxymethyl)quinolin-2-yl)acetamide (80). Compound **79** (0.732 g, 3.0 mmol) was diluted in anhydrous THF (10 mL) and cooled to −15 °C. LiAlH$_4$ (1 M in THF, 4.5 mL, 4.5 mmol) was added dropwise over 5 min, and the mixture was stirred for 1 h. The reaction was quenched by the addition of EtOAc (10 mL) and sat. aq. sodium potassium tartrate solution (20 mL) and stirred until two layers formed. The layers were separated, and the aqueous layer was extracted with EtOAc (4 × 50 mL). The organic phase was washed with sat. aq. NH$_4$Cl (50 mL), the aqueous phase was re-extracted with 20 mL of EtOAc following this wash, and the combined organic layers were washed with sat. aq. NaCl (50 mL), and dried over anhydrous sodium sulfate. Concentration afforded a white residue, which was precipitated from minimal EtOAc with hexanes to afford crude **80** as a white solid (0.433 g, 67%), which was used in the following step without further purification; ^{1}H NMR (500 MHz, CDCl$_3$) δ 8.41 (d, J = 8.9 Hz, 1 H), 8.32 (s, 1 H), 8.17 (d, J = 8.9 Hz, 1 H), 7.81 (s, 1 H), 7.79 (d, J = 8.3 Hz, 1 H), 7.47 (d, J = 8.3 Hz, 1 H), 4.91 (s, 2 H), 2.28 (s, 3 H); ^{13}C NMR (126 MHz, CDCl$_3$) δ 169.1, 151.1, 146.6, 143.1, 138.5, 127.9, 125.6, 124.5, 124.3, 114.0, 65.0, 25.0; ESIMS m/z (rel. intensity) 217 (MH$^+$, 100)

N-(7-Formylquinolin-2-yl)acetamide (81). Dess-Martin period-inane (0.869 g, 2.05 mmol) was diluted in anhydrous CH$_2$Cl$_2$ (25 mL), and alcohol **80** (0.364 g, 1.71 mmol) was added in one portion. The mixture was stirred at room temperature for 70 min and then quenched by the addition of sat. aq. Na$_2$S$_2$O$_3$ (15 mL). After being stirred for 15 min, the layers were separated, and the aqueous layer was extracted with CH$_2$Cl$_2$ (2 × 20 mL). The organic layers were washed with sat. aq. NaHCO$_3$ and sat. aq. NaCl (20 mL each). The organic layer was dried over anhydrous sodium sulfate and concentrated, and the residue was purified by flash column chromatography, eluting with a gradient of CH$_2$Cl$_2$ to 40% EtOAc in CH$_2$Cl$_2$, to yield **81** as a yellow amorphous solid (0.300 g, 82%); mp 199−200 °C. ^{1}H NMR (500 MHz; CDCl$_3$): δ 10.21 (d, J = 0.5 Hz, 1 H), 8.57 (br d, J = 9.0 Hz, 1 H), 8.29 (t, J = 0.7 Hz, 1 H), 8.25 (d, J = 9.0 Hz, 1 H), 7.96 (dd, J = 8.3, 1.4 Hz, 1 H), 7.92 (d, J = 8.4 Hz, 1 H), 2.32 (s, 3 H); the acetamidoquinoline N−H proton is broadened into the baseline ∼8.3 ppm. ^{13}C NMR (126 MHz; CDCl$_3$): δ 192.0, 151.9, 139.2, 137.7, 132.3, 129.8, 129.0, 122.6, 116.7, 26.1; one of the quinoline carbons is broadened into the baseline and is not visible; ESIMS m/z (rel. intensity) 215 (MH$^+$, 14).

Purified NOS Enzyme Assays. Rat and human nNOS, murine macrophage iNOS, bovine eNOS, and rat nNOS double mutant D597N/M336V were recombinant enzymes, expressed in *E. coli* and purified as previously reported.[49−51] To test for enzyme inhibition, the hemoglobin capture assay was used to measure nitric oxide production. The assay was performed at 37 °C in HEPES buffer (100 mM, with 10% glycerol, pH 7.4) in the presence of 10 μM L-arginine. Also included were 100 μM NADPH, 0.83 mM CaCl$_2$, approximately 320 units/mL of calmodulin, 10 μM H$_4$B, and human oxyhemoglobin (3 μM). For iNOS, CaCl$_2$ and calmodulin were omitted and replaced with HEPES buffer (as neither are required for activation of iNOS). The assay was performed in 96-well plates using a Synergy 4 BioTek hybrid reader, and the dispensing of NOS enzyme and hemoglobin were automated; after 30 s (maximum delay), NO production was read by monitoring the absorbance at 401 nm (resulting from the conversion of oxyhemoglobin to methemoglobin). Kinetic readouts were performed for 3 or 5 min. Each compound was assayed at least in duplicate, and seven to nine concentrations (500 μM−50 nM or 100 μM−10 nM for eNOS and iNOS; 50 μM to 5 nM for nNOS) were used to construct dose−response curves. IC$_{50}$ values were calculated by nonlinear regression using GraphPad Prism software, and K_i values were obtained using the Cheng−Prusoff equation[52] $[K_i = IC_{50}/(1 + [S]/K_m)]$ with the following K_m values: 1.3 μM (rat nNOS), 1.6 μM (human nNOS), 8.2 μM (murine macrophage iNOS), 1.7 μM (bovine eNOS), and 1.9 μM (rat nNOS D597N/M336V double mutant).[38]

Inhibitor Complex Crystal Preparation. The preparations of rat nNOS (wild type or D597N/M336V double mutant), bovine eNOS,

and human nNOS heme domains used for crystallographic studies were carried out using the procedures described previously.[42,53] The rat nNOS heme domain (WT or double mutant, at 9 mg/mL containing 20 mM histidine) or the bovine eNOS heme domain (at 10 mg/mL containing 2 mM imidazole) were used for the sitting drop vapor diffusion crystallization setup under conditions previously reported.[54,55] Human nNOS crystals were obtained with the triple K301R/R354A/G357D mutant heme domain sample at 10 mg/mL. By slightly modifying the original conditions[42] where the monoclinic C2 crystals grew, a new crystal form belonging to the $P2_12_12_1$ space group was obtained.[42] Fresh crystals (1−2 days old) were first passed stepwise through cryoprotectant solutions and then soaked with 10 mM inhibitor for 4−6 h at 4 °C before being flash cooled with liquid nitrogen.

X-ray Diffraction Data Collection, Data Processing, and Structural Refinement. The cryogenic (100 K) X-ray diffraction data were collected remotely at the Stanford Synchrotron Radiation Lightsource (SSRL) or Advanced Light Source (ALS) through the data collection control software Blu-Ice[56] and a crystal mounting robot. When a Q315r CCD detector was used, 100−125° of data were typically collected with 0.5° per frame. If a Pilatus pixel array detector was used, 140−160° of fine-sliced data were collected with 0.2° per frame. Raw CCD data frames were indexed, integrated, and scaled using HKL2000,[57] but the pixel array data were processed with XDS[58] and scaled with Scala (or Aimless).[59] The binding of inhibitors was detected by initial difference Fourier maps calculated with REFMAC.[60] The inhibitor molecules were then modeled in COOT[61] and refined using REFMAC or PHENIX.[62] Disordering in portions of inhibitors bound in the NOS active sites was often observed, sometimes resulting in poor density quality. However, partial structural features usually could still be visible if the contour level of the σA weighted $2m|F_o| − D|F_c|$ map dropped to 0.5 σ, which afforded the building of reasonable models into the disordered regions. Water molecules were added in REFMAC and checked by COOT. The TLS[63] protocol was implemented in the final stage of refinements with each subunit as one TLS group. The omit $F_o − F_c$ density maps were calculated by removing inhibitor coordinates from the input PDB file before running one more round of TLS refinement in REFMAC or in PHENIX (simulated annealing protocol with a 2000 K initial temperature). The resulting map coefficients DELFWT and PHDELWT were used to generate maps. The refined structures were validated in COOT before deposition in the RCSB protein data bank. The crystallographic data collection and structure refinement statistics are summarized in Table S1, with the PDB accession codes included.

Caco-2 Permeability Assay. Caco-2 monolayer assays were performed by Cyprotex US, LLC (Watertown, MA) using the following standard procedure: Caco-2 cells, grown in tissue culture flasks, were trypsinized, resuspended, and grown and differentiated in 96-well plates for 3 weeks; monolayer formation was determined by measuring the transport of Lucifer yellow, an impermeable dye. All assays were performed at a concentration of 10 μM for 2 h. For apical to basolateral (A → B) permeability, compounds were added on the apical side (A), with permeation determined at the receiving (basolateral, B) side, where the receiving buffer was removed for analysis by LC/MS/MS using an Agilent 6410 mass spectrometer (ESI, MRM mode) coupled with an Agilent 1200 HPLC, using propranolol as an analytical internal standard. Buffers used were 100 μM Lucifer yellow in transport buffer (1.98 g/L glucose in 10 mM HEPES, 1× Hank's Balanced Salt Solution, pH 6.5) (apical side) and transport buffer at pH 7.4 (basolateral side). Apparent permeability (P_{app}) is expressed using the following equation: $P_{app} = (dQ/dt)/C_0A$, where the numerator is the rate of permeation, C_0 is initial concentration, and A is the monolayer area (0.11 cm^2). For bidirectional permeability, the efflux ratio was defined as P_{app} (B → A)/P_{app} (A → B); high efflux ratio values (>3) indicate that a compound may be a substrate for P-gp or other active transport systems.

ASSOCIATED CONTENT

Supporting Information

The Supporting Information is available free of charge on the ACS Publications website at DOI: 10.1021/acs.jmedchem.5b01330.

> Crystallographic data collection and refinement statistics for rat and human nNOS, eNOS, and nNOS double mutant crystal structures; synthesis and analytical data for compounds 28−59; and rnNOS-10, eNOS-7, -8, -17, -20, and hnNOS-17 crystal structures (PDF)
>
> SMILES data (CSV)

Accession Codes

PDB codes for X-ray crystal structures described in this study have been deposited in the Protein Data Bank under the following accession codes: 5AD4, 5AD5, 5AD6, 5AD6, 5AD8, 5AD9, 5ADA, 5ADB, 5ADC, 5ADD, 5ADE, 5ADF, 5ADG, 5ADI, 5ADJ, 5ADK, 5ADL, 5ADN, 5FJ2, and 5FJ3.

AUTHOR INFORMATION

Corresponding Authors

*(T.L.P.) Tel: +1 949 824 7020. E-mail: poulos@uci.edu.

*(R.B.S.) Tel:+1 847 491 5653. Fax: +1 847 491 7713. E-mail: Agman@chem.northwestern.edu.

Notes

The authors declare no competing financial interest.

ACKNOWLEDGMENTS

ABBREVIATIONS USED

NOS, neuronal nitric oxide synthase; iNOS, inducible nitric oxide synthase; eNOS, endothelial nitric oxide synthase; FMN, flavin mononucleotide; H4B, (6R)-5,6,7,8-tetrahydrobiopterin; tPSA, total polar surface area; P_{app}, apparent permeability; HEPES, 4-(2-hydroxyethyl)-1-piperazineethanesulfonic acid; PDSP, psychoactive drug screening program; WT, wild-type

REFERENCES

(1) Hobbs, A.; Higgs, A.; Moncada, S. Inhibition of nitric oxide synthase as a potential therapeutic target. *Annu. Rev. Pharmacol. Toxicol.* **1999**, *39*, 191−220.

(2) Förstermann, U.; Sessa, W. C. Nitric oxide synthases: regulation and function. *Eur. Heart J.* **2012**, *33*, 829−837.

(3) Torreilles, F.; Salman-Tabcheh, S.; Guerin, M.; Torreilles, J. Neurodegenerative disorders: the role of peroxynitrite. *Brain Res. Rev.* **1999**, *30*, 153−163.

(4) Uehara, T.; Nakamura, T.; Yao, D.; Shi, Z. Q.; Gu, Z.; Ma, Y.; Masliah, E.; Nomura, Y.; Lipton, S. A. S-Nitrosylated protein-disulphide isomerase links protein misfolding to neurodegeneration. *Nature* **2006**, *441*, 513−517.

(5) Zhang, L.; Dawson, V. L.; Dawson, T. M. Role of nitric oxide in Parkinson's disease. *Pharmacol. Ther.* **2006**, *109*, 33−41.

(6) Dorheim, M.-A.; Tracey, W. R.; Pollock, J. S.; Grammas, P. Nitric oxide synthase activity is elevated in brain microvessels in Alzheimer's disease. *Biochem. Biophys. Res. Commun.* **1994**, *205*, 659−665.

(7) Drechsel, D. A.; Estevez, A. G.; Barbeito, L.; Beckman, J. S. Nitric oxide-mediated oxidative damage and the progressive demise of motor neurons in ALS. *Neurotoxic. Res.* **2012**, *22*, 251−264.

(8) Huang, Z.; Huang, P. L.; Panahian, N.; Dalkara, T.; Fishman, M. C.; Moskowitz, M. A. Effects of cerebral ischemia in mice deficient in neuronal nitric oxide synthase. *Science* **1994**, *265*, 1883−1885.

(9) Hantraye, P.; Brouillet, E.; Ferrante, R.; Palfi, S.; Dolan, R.; Matthews, R. T.; Beal, M. F. Inhibition of neuronal nitric oxide synthase prevents MPTP-induced Parkinsonism in baboons. *Nat. Med.* **1996**, *2*, 1017−1021.

(10) Watanabe, Y.; Kato, H.; Araki, T. Protective action of neuronal nitric oxide synthase inhibitor in the MPTP mouse model of Parkinson's disease. *Metab. Brain Dis.* **2008**, *23*, 51−69.

(11) Ikeda, K.; Iwasaki, Y.; Kinoshita, M. Neuronal nitric oxide synthase inhibitor, 7-nitroindazole, delays motor dysfunction and spinal motoneuron degeneration in the wobbler mouse. *J. Neurol. Sci.* **1998**, *160*, 9−15.

(12) Siddhanta, U.; Presta, A.; Fan, B.; Wolan, D.; Rousseau, D. L.; Stuehr, D. J. Domain swapping in inducible NO synthase: electron transfer cccurs between flavin and heme groups located on adjacent subunits in the dimer. *J. Biol. Chem.* **1998**, *273*, 18950−18958.

(13) Rosen, G. M.; Tsai, P.; Pou, S. Mechanism of free-radical generation by nitric oxide synthase. *Chem. Rev.* **2002**, *102*, 1191−1199.

(14) Alderton, W. K.; Cooper, C. E.; Knowles, R. G. Nitric oxide synthases: structure, function and inhibition. *Biochem. J.* **2001**, *357*, 593−615.

(15) Mukherjee, P.; Cinelli, M. A.; Kang, S.; Silverman, R. B. Development of nitric oxide synthase (NOS) inhibitors for neurodegenerative diseases and neuropathic pain. *Chem. Soc. Rev.* **2014**, *43*, 6814−6838.

(16) Kobayashi, Y.; Ikeda, K.; Shinozuka, K.; Nara, Y.; Yamori, Y.; Hattori, K. L-nitroarginine increases blood pressure in the rat. *Clin. Exp. Pharmacol. Physiol.* **1991**, *18*, 397−399.

(17) Seelig, A. The role of size and charge for blood-brain barrier permeation of drugs and fatty acids. *J. Mol. Neurosci.* **2007**, *33*, 32−41.

(18) Cinelli, M. A.; Li, H.; Chreifi, G.; Martásek, P.; Roman, L. J.; Poulos, T. L.; Silverman, R. B. Simplified 2-aminoquinoline-based scaffold for potent and selective neuronal nitric oxide synthase inhibition. *J. Med. Chem.* **2014**, *57*, 1513−1530.

(19) Besnard, J.; Ruda, G. F.; Setola, V.; Abecassis, K.; Rodriguiz, R. M.; Huang, X. P.; Norval, S.; Sassano, M. F.; Shin, A. I.; Webster, L. A.; Simeons, F. R.; Stojanovski, L.; Prat, A.; Seidah, N. G.; Constam, D. B.; Bickerton, G. R.; Read, K. D.; Wetsel, W. C.; Gilbert, I. H.; Roth, B. L.; Hopkins, A. L. Automated design of ligands to polypharmacological profiles. *Nature* **2012**, *492*, 215−220.

(20) Klabunde, T.; Evers, A. GPCR antitarget modeling: pharmacophore models for biogenic amine binding GPCRs to avoid GPCR-mediated side effects. *ChemBioChem* **2005**, *6*, 876−889.

(21) Lowe, J. A., III; Qian, W.; Volkmann, R. A.; Heck, S.; Nowakowski, J.; Nelson, R.; Nolan, C.; Liston, D.; Ward, K.; Zorn, S.; Johnson, C.; Vanase, M.; Faraci, W. S.; Verdries, K. A.; Baxter, J.; Doran, S.; Sanders, M.; Ashton, M.; Whittle, P.; Stefaniak, M. A new class of selective and potent inhibitors of neuronal nitric oxide synthase. *Bioorg. Med. Chem. Lett.* **1999**, *9*, 2569−2572.

(22) Lowe, J. A., III; Qian, W.; Drozda, S. E.; Volkmann, R. A.; Nason, D.; Nelson, R. B.; Nolan, C.; Liston, D.; Ward, K.; Faraci, S.; Verdries, K.; Seymour, P.; Majchrzak, M.; Villalobos, A.; White, W. F. Structure-activity relationships of potent, selective inhibitors of neuronal nitric oxide synthase based on the 6-phenyl-2-aminopyridine structure. *J. Med. Chem.* **2004**, *47*, 1575−1586.

(23) Nason, D. M.; Heck, S. D.; Bodenstein, M. S.; Lowe, J. A., III; Nelson, R. B.; Liston, D. R.; Nolan, C. E.; Lanyon, L. F.; Ward, K. M.; Volkmann, R. A. Substituted 6-phenyl-pyridin-2-ylamines: selective and potent inhibitors of nitric oxide synthase. *Bioorg. Med. Chem. Lett.* **2004**, *14*, 4511−4514.

(24) Ramnauth, J.; Renton, P.; Dove, P.; Annedi, S. C.; Speed, J.; Silverman, S.; Mladenova, G.; Maddaford, S. P.; Zinghini, S.; Rakhit, S.; Andrews, J.; Lee, D. K. H.; Zhang, D.; Porreca, F. 1,2,3,4-Tetrahydroquinoline-based selective human neuronal nitric oxide synthase (nNOS) inhibitors: lead optimization studies resulting in the identification of *N*-(1-(2-(methylamino)ethyl)-1,2,3,4-tetrahydroquinolin-6-yl)thiophene-2-carboximidamide as a preclinical development Candidate. *J. Med. Chem.* **2012**, *55*, 2882−2983.

(25) Annedi, S. C.; Ramnauth, J.; Maddaford, S. P.; Renton, P.; Rakhit, S.; Mladenova, G.; Dove, P.; Silverman, S.; Andrews, J. S.; Felice, M. D.; Porreca, F. Discovery of cis-*N*-(1-(4-(Methylamino)-cyclohexyl)indolin-6-yl)thiophene-2-carboximidamide: A 1,6-disubstituted indoline derivative as a highly selective inhibitor of human neuronal nitric oxide synthase (nNOS) without any cardiovascular liabilities. *J. Med. Chem.* **2012**, *55*, 943−955.

(26) Flinspach, M.; Li, H.; Jamal, J.; Yang, W.; Huang, H.; Hah, J.-M.; Gomez-Vidal, J. A.; Litzinger, E. A.; Silverman, R. B.; Poulos, T. L. Structural basis for dipeptide amide isoform-selective inhibition of neuronal nitric oxide synthase. *Nat. Struct. Mol. Biol.* **2004**, *11*, 54−59.

(27) Kang, S.; Tang, W.; Li, H.; Chreifi, G.; Martasek, P.; Roman, L. J.; Poulos, T. L.; Silverman, R. B. Nitric oxide synthase inhibitors that interact with both heme propionate and tetrahydrobiopterin show high isoform selectivity. *J. Med. Chem.* **2014**, *57*, 4382−4396.

(28) Xue, F.; Li, H.; Fang, J.; Roman, L. J.; Martasek, P.; Poulos, T. L.; Silverman, R. B. Peripheral but crucial: A hydrophobic pocket (Tyr706, Leu337, and Met336) for potent and selective inhibition of neuronal nitric oxide synthase. *Bioorg. Med. Chem. Lett.* **2010**, *20*, 6258−6261.

(29) Inglis, S.; Jones, R.; Fritz, D.; Stojkoski, C.; Booker, G.; Pyke, S. Synthesis of 5-, 6- and 7-substituted-2-aminoquinolines as SH3 domain ligands. *Org. Biomol. Chem.* **2005**, *3*, 2543−2557.

(30) Kóródi, F. A simple new synthetic method for the preparation of 2-aminoquinolines. *Synth. Commun.* **1991**, *21*, 1841−1846.

(31) Smith, J. A.; Jones, R. K.; Booker, G. W.; Pyke, S. M. Sequential and selective Buchwald-Hartwig amination reactions for the controlled functionalization of 6-bromo-2-chloroquinoline: synthesis of ligands for the Tec Src homology 3 domain. *J. Org. Chem.* **2008**, *73*, 8880−8892.

(32) Sun, W.; Blanton, M. P.; Gabriel, J. L.; Canney, D. J. Bioisosteric replacement in the design and synthesis of ligands for nicotinic acetylcholine receptors. *Med. Chem. Res.* **2005**, *14*, 241−259.

(33) Romera, J. L.; Cid, J. M.; Trabanco, A. Potassium iodide catalysed monoalkylation of anilines under microwave radiation. *Tetrahedron Lett.* **2004**, *45*, 8797−8800.

(34) Shin, G.-J.; Moon, J. Y.; Bae, A. N.; Kim, E. G.; Seo, S. H. Preparation of quinolinecarboxylic acid-amide derivatives as Fab I inhibitors. *Repub. Korean Kongkae Taeho Kongbo* **2009**; KR20090063869.

(35) Labby, K. J.; Xue, F.; Kraus, J. M.; Ji, H.; Mataka, J.; Li, H.; Martásek, P.; Roman, L. J.; Poulos, T. L.; Silverman, R. B. Intramolecular hydrogen bonding: A potential strategy for more bioavailable inhibitors of neuronal nitric oxide synthase. *Bioorg. Med. Chem.* **2012**, *20*, 2435−2443.

(36) Hevel, J. M.; Marletta, M. A. Nitric-oxide synthase assays. *Methods Enzymol.* **1994**, *233*, 250−258.

(37) Delker, S. L.; Ji, H.; Li, H.; Jamal, J.; Fang, J.; Xue, F.; Silverman, R. B.; Poulos, T. L. Unexpected binding modes of nitric oxide synthase

inhibitors effective in the prevention of cerebral palsy. *J. Am. Chem. Soc.* **2010**, *132*, 5437−5442.

(38) Delker, S. L.; Xue, F.; Li, H.; Jamal, J.; Silverman, R. B.; Poulos, T. L. Role of zinc in isoform-selective inhibitor binding to neuronal nitric oxide synthase. *Biochemistry* **2010**, *49*, 10803−10810.

(39) Mukherjee, P.; Li, J.; Sevrioukova, I.; Chreifi, G.; Martasek, P.; Roman, L. J.; Poulos, T. L.; Silverman, R. B. Novel 2,4-disubstituted pyrimidines as potent, selective, and cell-permeable inhibitors of neuronal nitric oxide synthase. *J. Med. Chem.* **2015**, *58*, 1067−1088.

(40) Huang, H.; Li, H.; Martasek, P.; Roman, L. J.; Poulos, T. J.; Silverman, R. B. Structure-guided design of selective inhibitors of neuronal nitric oxide synthase. *J. Med. Chem.* **2013**, *56*, 3024−3032.

(41) Fedorov, R.; Vasan, R.; Ghosh, D. K.; Schlichting, I. Structures of nitric oxide synthase isoforms complexed with the inhibitor AR-R17477 suggest a rational basis for specificity and inhibitor design. *Proc. Natl. Acad. Sci. U. S. A.* **2004**, *101*, 5892−5897.

(42) Kang, S.; Li, H.; Tang, W.; Martásek, P.; Roman, L. J.; Poulos, T. L.; Silverman, R. B. 2-Aminopyridines with a truncated side chain to improve human neuronal nitric oxide synthase inhibitory potency and selectivity. *J. Med. Chem.* **2015**, *58*, 5548−5560.

(43) Li, H.; Jamal, J.; Plaza, C.; Pineda, S. H.; Chreifi, G.; Jing, Q.; Cinelli, M. A.; Silverman, R. B.; Poulos, T. L. Crystal structures of human constitutive nitric oxide synthases. *Acta Crystallogr., Sect. D: Biol. Crystallogr.* **2014**, *70*, 2667−2674.

(44) Lohmann, C.; Huwel, S.; Galla, H. J. Predicting blood-brain barrier permeability of drugs: evaluation of different in vitro assays. *J. Drug Targeting* **2002**, *10*, 263−276.

(45) Stewart, B. H.; Chan, O. H.; Lu, R. H.; Reyner, E. L.; Shmid, H. L.; Hamilton, H. W.; Steinbaugh, B. A.; Taylor, M. D. Comparison of intestinal permeabilities determined in multiple *in vitro* and *in situ* models: relationship to absorption in humans. *Pharm. Res.* **1995**, *12*, 693−699.

(46) Hazeldine, S. T.; Polin, L.; Kushner, J.; White, K.; Bouregeois, N. M.; Crantz, B.; Palomino, E.; Corbett, T. H.; Horwitz, J. P., II Synthesis and biological evaluation of some bioisosteres and congeners of the antitumor agent, 2-{4-[(7-chloro-2-quinoxalinyl)oxy]phenoxy}-propionic acid (XK469). *J. Med. Chem.* **2002**, *45*, 3130−3137.

(47) Hartmann, R.; Marchais-Oberwinkler, S.; Xu, K.; Werth, R. Biaryl Derivatives as Selective 17-Beta-hydroxysteroid Dehydrogenase Type 2 Inhibitors. US20140057953 A1, Feb 27th, 2014.

(48) Nhu, D.; Duffy, S.; Avery, V. M.; Hughes, A.; Baell, J. B. Antimalarial 3-arylamino-5-benzylamino-1,2,4,5-tetrazines. *Bioorg. Med. Chem. Lett.* **2010**, *20*, 4496−4498.

(49) Roman, L. J.; Sheta, E. A.; Martásek, P.; Gross, S. S.; Liu, Q.; Masters, B. S. S. High-level expression of functional rat neuronal nitric oxide synthase in *Escherichia coli*. *Proc. Natl. Acad. Sci. U. S. A.* **1995**, *92*, 8428−8432.

(50) Hevel, J. M.; White, K. A.; Marletta, M. A. Purification of the inducible murine macrophage nitric oxide synthase: identification as a flavoprotein. *J. Biol. Chem.* **1991**, *266*, 22789−22791.

(51) Gerber, N. C.; Ortiz de Montellano, P. R. Neuronal nitric oxide synthase: expression in *Escherichia coli*, irreversible inhibition by phenyldiazene, and active site topology. *J. Biol. Chem.* **1995**, *270*, 17791−17796.

(52) Cheng, Y.-C.; Prusoff, W. H. Relationship between the inhibition constant (K_i) and the concentration of the inhibitor which causes 50% inhibition (IC50) of an enzymatic reaction. *Biochem. Pharmacol.* **1973**, *22*, 3099−3108.

(53) Li, H.; Jamal, J.; Delker, S.; Plaza, C.; Ji, H.; Jing, Q.; Huang, H.; Kang, S.; Silverman, R. B.; Poulos, T. L. The mobility of a conserved tyrosine residue controls isoform-dependent enzyme-inhibitor inter-action in nitric oxide synthases. *Biochemistry* **2014**, *53*, 5272−5279.

(54) Li, H.; Shimizu, H.; Flinspach, M.; Jamal, J.; Yang, W.; Xian, M.; Cai, T.; Wen, E. Z.; Jia, Q.; Wang, P. G.; Poulos, T. L. The novel binding mode of *N*-alkyl-*N*′-hydroxyguanidine to neuronal nitric oxide synthase provides mechanistic insights into NO biosynthesis. *Biochemistry* **2002**, *41*, 13868−13875.

(55) Raman, C. S.; Li, H.; Martásek, P.; Král, V.; Masters, B. S. S.; Poulos, T. L. Crystal structure of constitutive endothelial nitric oxide

synthase: a paradigm for pterin function involving a novel metal center. *Cell* **1998**, *95*, 939−950.

(56) McPhillips, T. M.; McPhillips, S. E.; Chiu, H. J.; Cohen, A. E.; Deacon, A. M.; Ellis, P. J.; Garman, E.; Gonzalez, A.; Sauter, N. K.; Phizackerley, R. P.; Soltis, S. M.; Kuhn, P. Blu-Ice and the Distributed Control System: software for data acquisition and instrument control at macromolecular crystallography beamlines. *J. Synchrotron Radiat.* **2002**, *9*, 401−406.

(57) Otwinowski, Z.; Minor, W. Processing of X-ray diffraction data collected in oscillation mode. *Methods Enzymol.* **1997**, *276*, 307−326.

(58) Kabsch, W. XDS. *Acta Crystallogr., Sect. D: Biol. Crystallogr.* **2010**, *66*, 125−132.

(59) Evans, P. R. Scaling and assessment of data quality. *Acta Crystallogr., Sect. D: Biol. Crystallogr.* **2006**, *62*, 72−82.

(60) Murshudov, G. N.; Vagin, A. A.; Dodson, E. J. Refinement of macromolecular structures by the maximum-likelihood method. *Acta Crystallogr., Sect. D: Biol. Crystallogr.* **1997**, *53*, 240−255.

(61) Emsley, P.; Cowtan, K. Coot: model-building tools for molecular graphics. *Acta Crystallogr., Sect. D: Biol. Crystallogr.* **2004**, *60*, 2126−2132.

(62) Adams, P. D.; Afonine, P. V.; Bunkóczi, G.; Chen, V. B.; Davis, I. W.; Echols, N.; Headd, J. J.; Hung, L.-W.; Kapral, G. J.; Grosse-Kunstleve, R. W.; McCoy, A. J.; Moriarty, N. W.; Oeffner, R.; Read, R. J.; Richardson, D. C.; Richardson, J. S.; Terwilliger, T. C.; Zwart, P. H. PHENIX: a comprehensive Python-based system for macromolecular structure solution. *Acta Crystallogr., Sect. D: Biol. Crystallogr.* **2010**, *66*, 213−221.

(63) Winn, M. D.; Isupov, M. N.; Murshudov, G. N. Use of TLS parameters to model anisotropic displacements in macromolecular refinement. *Acta Crystallogr., Sect. D: Biol. Crystallogr.* **2001**, *57*, 122−133.